NOAA TECHNICAL MEMORANDUM ERL PMEL-107

CORRECTING MOORED ADCP DATA FOR FISH-BIAS ERRORS AT 0°, 110°W AND 0°, 140°W FROM 1990 TO 1993

Patricia E. Plimpton
H. Paul Freitag
Michael J. McPhaden

Pacific Marine Environmental Laboratory
7600 Sand Point Way NE
Seattle, Washington

April 1995

Contribution No. 1586 from NOAA/Pacific Marine Environmental Laboratory

NOTICE

Mention of a commercial company or product does not constitute an endorsement by NOAA/ERL. Use of information from this publication concerning proprietary products or the tests of such products for publicity or advertising purposes is not authorized.

Contribution No. 1586 from NOAA/Pacific Marine Environmental Laboratory

For sale by the National Technical Information Service, 5285 Port Royal Road
Springfield, VA 22161

CONTENTS

Page

Correcting Moored ADCP Data for Fish-bias Errors at 0°, 110°W and 0°, 140°W From 1990 to 1993

Patricia E. Plimpton, H. Paul Freitag, and Michael J. McPhaden

ABSTRACT. This report describes the processing techniques utilized in producing daily averaged velocity profiles from downward-looking RDI Acoustic Doppler Current Profilers (ADCPs) mounted on surface moorings at 0°, 110°W and 0°, 140°W. The data presented are from 1991 to 1993 at 110°W and 1990 to 1993 at 140°W. Initial post-processing corrections include bin depth adjustments using historical sound velocity profiles, and current velocity adjustments using in situ temperature to estimate surface sound velocity. Of greater significance are the velocity corrections required due to the presence of pelagic fish in the vicinity of the moorings. The ADCP velocities are compared with mechanical current meters (MCMs) set at specific depths in the mooring line. This comparison indicates that the ADCP speeds are, at times, biased towards lower values due to the reflection of acoustic energy from fish. After computing a mean ADCP–MCM offset for each deployment, an empirical orthogonal function (EOF) analysis is applied to the time-varying ADCP–MCM differences. For the mean and each eigenmode, differences computed at the MCM depths are interpolated to the finer vertical resolution of the ADCP depth grid. The vertically interpolated amplitudes from the mean and the first three eigenmodes are used to produce a correction for the ADCP speeds. The ADCP current directions do not appear affected by the presence of fish and are used, along with the corrected ADCP speeds, to produce a significantly more accurate data base of daily averaged zonal and meridional velocity profiles.

1. Introduction

Current meter moorings with telemetering 153.6 kHz RD Instruments (RDI) acoustic Doppler current profilers (ADCPs) have been deployed on the equator in the eastern equatorial Pacific since 1990 as part of the Tropical Ocean-Global Atmosphere (TOGA) Program and NOAA's Equatorial Pacific Ocean Climate Studies (EPOCS) Program. These moorings, referred to as PROTEUS (PROfile TElemetry of Upper ocean currentS) moorings (McPhaden *et al.*, 1990), are embedded in the TOGA Tropical Atmosphere Ocean (TAO) Array (Figure 1) of nearly 70 wind and thermistor chain moorings spanning the width of the tropical Pacific from 8°N–8°S, 95°W–137°E (Hayes *et al.*, 1991; McPhaden, 1993). The purpose of the TAO Array is to provide high quality surface wind, temperature and ocean current data on a basin scale in real-time to support short-term climate studies, most notably those related to the El Niño/Southern Oscillation (ENSO) phenomenon. Current meter moorings in the TAO Array provide direct estimates of velocity at the equator where geostrophy does not apply and where ocean dynamics is a crucial determinant in the evolution of ENSO sea surface temperature anomalies. PROTEUS data are stored internally as hourly values, and are also processed on board to daily averages for transmission to shore via Service Argos.

This report describes the accuracies and errors of current measurements from the RDI ADCPs on the equator at 110°W and 140°W. Mechanical current meters (MCMs) have been used to collect current measurements at these sites since 1979 at 110°W and 1983 at 140°W. Whereas the MCMs measure current velocities at only 6 or 7 specific depths, the ADCP velocities are collected with a much finer vertical resolution. The ADCP measurements represent a weighted average over 16 m

and are available at 8-m depth intervals. Unfortunately, the presence of pelagic fish (Freitag *et al.*, 1992), which are at times attracted to the vicinity of the moorings, can result in large velocity errors in the ADCP data. Techniques are presented here to correct the ADCP velocities using the MCM data. The corrected profiles are both highly resolved in the vertical and relatively free of data gaps, thus representing an optimal blend of MCM and ADCP data. Corrections have not been made to the PROTEUS mooring time series at 0°, 156°E and 0°, 165°E since these sites are relatively free of the fish bias errors seen further to the east at 0°, 110°W and 0°, 140°W (Freitag *et al.*, 1993).

2. PROTEUS Data Collection and Processing

The PROTEUS moorings were recovered and redeployed on a 5–7 month schedule (Table 1). The downward-looking 153.6 kHz ADCPs were set to collect data with 8-m bin and pulse lengths, at a 1-second sample rate for 6 minutes centered at the top of the hour. Early deployments were set to use a narrow low pass filter bandwith (300 Hz) for the entire depth profile, resulting in some skew error (Pullen *et al.*, 1992). Beginning in Fall 1991, a broad bandwidth filter (600 Hz) was used in the shallower portion of the depth profile, switching to a narrow bandwidth filter at a depth below the core of the Undercurrent. The ADCPs were equipped with a KVH compass calibrated at PMEL to an accuracy of ±2.5°.

The ADCP velocities were collected assuming a surface sound speed of 1536 m s^{-1}. Hourly surface sound speeds computed from in situ temperatures measured at the transducer head and historically averaged surface salinities (34.7% at 110°W and 35.1% at 140°W) were used to

Table 1. PROTEUS Mooring Deployments at 0°, 110°W and 0°, 140°W.

	Latitude	Longitude	Start Date	End Date
		140°W Sites		
PR01	0° 0.3′N	139° 55.8′W	1 May 90	24 Oct 90
PR02	0° 0.4′S	140° 11.4′W	28 Oct 90	6 May 91
PR03	0° 0.6′N	140° 2.6′W	9 May 91	6 Nov 91
PR05	0° 1.3′N	140° 2.3′W	10 Nov 91	28 Apr 92
PR07	0° 2.0′N	139° 59.8′W	1 May 92	12 Sep 92
PR09	0° 2.1′N	139° 59.9′W	16 Sep 92	25 Apr 93
PR11	0° 3.2′N	139° 59.4′W	28 Apr 93	11 Oct 93
PR11a	0° 0.7′S	139° 52.6′W	28 Apr 93	11 Oct 93
		110°W Sites		
PR04	0° 2.2′N	110° 0.3′W	17 May 91	26 Oct 91
PR06	0° 0.4′S	109° 58.6′W	30 Oct 91	11 May 92
PR08	0° 3.7′N	110° 2.4′W	14 May 92	3 Nov 92
PR10	0° 1.4′N	109° 57.8′W	6 Nov 92	7 May 93
PR12	0° 1.4′N	109° 57.8′W	9 May 93	8 Sep 93

correct the ADCP velocities (Anonymous, RD Primer, 1989). In situ sound velocity profiles were not available, so the nominal ADCP depth bin lengths, which assumed a constant sound speed with depth of 1475.1 m s^{-1}, were adjusted using historical hydrographic data. Mean sound velocities and standard deviations were computed from 41 CTDs at 110°W and 23 CTDs at 140°W. Figures 2a and 2b show the ADCP depth error for uncorrected profiles based on these computations. Mean errors grow to about 8 m at a depth of 300 m at both locations. However, the variations in the depth error are relatively small (i.e., 2 standard deviations are about ±25% of the mean, or a maximum of ±2 m at 300 m). Thus, once profiles are adjusted for the mean errors in Figures 2a and 2b, residual depth uncertainty is significantly less than the 8-m bin width of the measurements.

For comparison, MCMs were placed in the mooring lines at 6 or 7 depths between 3 m and 300 m. The MCMs were either EG&G Vector Averaging Current Meters (VACMs) or Vector Measuring Current Meters (VMCMs). Tow tank runs performed on VACMs at PMEL indicate that the rotor is accurate to within 1.2 cm s^{-1} in steady flow. While the absolute accuracy of a surface-moored VACM is unknown, there is evidence that it overestimates current velocity in highly variable flows (Beardsley, 1987; Karweit, 1974). Nevertheless, the VACM gives results similar to those of the VMCM, which has been found to underestimate velocity by a few percent in highly variable reversing flows (Weller and Davis, 1980). In comparisons of VACM/VMCM pairs separated by 1 m on taut-line equatorial moorings, Halpern (1987) found RMS differences of 7.4 cm s^{-1} (equal to about 10–12 percent of the mean speed) at 13–14 m and 3.5 cm s^{-1} (equal to about 5 percent of the mean speed) at 160–161 m. During pre-deployment checkout, VACM mechanical compass linearity (compass error relative to a chosen fixed direction) is confirmed to be ±5.6° or less, but absolute accuracy is undetermined. The VMCM flux gate compasses are calibrated relative to a PMEL standard, and are found accurate to ±2.5°.

In some deployments, the MCM at a specific depth failed before recovery. The MCM depths and coverage for each deployment are shown in Figures 3a and 3b. At 140°W, the PR03 10-m data was filled by linear interpolation between 3-m and 25-m data. The other missing 10-m data, PR02 and PR09, were filled by determining regression coefficients between 10-m and 25-m data from deployments without data gaps at these depths. Multiple linear regression formulae based on 10-m, 25-m and 45-m time series were used to fill the PR05 25-m data gaps. Similarly, regression formulae based on 25-m, 45-m and 80-m time series were used to fill the 45-m data gaps in the PR03 and PR09 records. Statistics derived from a comparison of the computed speeds at 10 m, 25 m, and 45 m with existing speeds at these depths provide confidence in this technique for filling missing MCM data (Table 2). The multiple linear regression technique using data from neighboring depths was less accurate for filling the 120-m data gaps in PR05 and PR06 (Table 2). However, for both PR05 and PR06, the fish bias errors appeared to be diurnally modulated as described in Freitag *et al.* (1993). Hence, daily averages for 120 m were computed using ADCP data from the portion of the day that was minimally affected by fish (2000 to 0200 local time). In one deployment (PR02),

Table 2. Comparison statistics between existing speeds and speeds computed with regression formulae. Regression fills for gaps at 120 m were not used because of the relatively low correlation at that depth. See text for discussion.

Depth (m)	Correlation Coefficient	RMS Difference (cm s^{-1})
10	.98	6.7
25	.99	3.0
45	.89	8.7
120	.63	19.4

data from a nearby subsurface ADCP mooring 8 km to the northeast (Weisberg *et al.*, 1991) were used to correct MCM speeds because of evidence of biofouling on the MCM rotors. The MCM data were corrected using regression formulae based on time series between the subsurface ADCP data and MCM data from the first 2.5 months of the deployment. In two cases (6 November 1992 to 7 May 1993 at 110°W, and 13–25 April 1993 at 140°W) MCM data gaps could not be filled.

3. ADCP Speed Bias

ADCPs are widely used to measure ocean velocities from bottom-mounted, moored and ship-mounted systems. The RDI ADCP is a four-beam system which transmits an acoustic signal, measures the Doppler shift of the oceanic backscatter as a function of time, and computes the beam-direction velocity component as a function of depth. The frequency shift of the return signal is caused by oceanic scatterers, consisting of small particles or zooplankton, whose motion is assumed to be due, on the average, to oceanic advection. In most cases, the assumption of scatterers advected passively by water motion is valid. However, pelagic fish are at times attracted to the vicinity of moorings. The presence of these fish or other sound scatterers, whose mean movement is not due to oceanic advection, will bias the velocity measurement (Freitag *et al.*, 1992; Wilson and Firing, 1992). For example, if a fish is detected in one ADCP beam but not the opposing beam, the measured horizontal velocity from the two beams would be equal to the average of the fish velocity and the ocean current. If fish congregate around a mooring in the presence of a non-zero current, their velocity (lower on the average than the ocean current) would dominate the signal and the ensemble averaged measurement of horizontal velocities would be biased low. In addition, the same fish could be detected in the side lobes of opposing beams. If these side lobe signals are much stronger than signals in the main lobe from the surrounding water, the horizontal velocity would tend towards zero. This is because the strong sidelobe signals in opposing beams would tend to cancel in the computation of horizontal velocity.

The presence of fish in the acoustic signal was evaluated using the ADCP echo intensity (EI), which is a function of the intensity of the backscattered acoustic signal. The strength of the backscattered signal in the four beams tended to vary with the diurnal movements of the zooplankton, hence the absolute EI values in the four beams could not be used to indicate the

presence of pelagic fish. However, Freitag *et al.* (1992) found that times of large horizontal velocity errors were coincident with times of large differences in beam-to-beam EI. Thus we computed the difference between the highest beam EI and the lowest beam EI, or the echo intensity range (EIR), as an indication of the presence of fish. Use of the EIR to determine the presence of fish is most effective when fish are detected in only one to three beams during the averaging interval, as in Freitag *et al.* (1992). EIR magnitudes would be reduced in cases where fish were detected in all four beams during the averaging period because the EI would be elevated to approximately the same levels in all beams.

Figures 4 and 5 show daily averaged data from equatorial deployments at 110°W from May 1991 to September 1993 and at 140°W from May 1990 to October 1993. Deployment and recovery times are shown by the black dots at the abscissas. Data are shown at the depths of the MCMs. ADCP speed data at 10 m depth have been estimated by linear extrapolation based on vertical gradients between bin 1 and bin 2. The solid lines are the ADCP–MCM daily speed differences. Missing data occur where MCM data, lost due to instrument failure, could not be filled. Periods of fish-biased data are clearly evident, with ADCP–MCM daily speed differences as large as 80 cm s^{-1}. Also shown are daily averages of echo intensity range. The evidence of fish bias in the ADCP data is highly correlated with times of increased echo intensity range, although there is not a simple relationship between the magnitude of the fish bias and the magnitude of the echo intensity range (Freitag *et al.*, 1993).

The moored ADCP data are collected as 6-minute averages, so individual pings with high echo intensity range could not be eliminated in post-processing. After the fish bias problem was identified, RDI created an algorithm to eliminate pings with large intensity range as an attempt to remove fish-biased data on a single-ping basis before averaging. The algorithm has been deployed at both locations for all deployments from early 1992 to the present, except for PR11 at 140°W (April–October, 1993). The algorithm did remove some fish-biased data, as determined by the percent good data per 6-minute ensemble, although large bias errors still remained (Freitag *et al.*, 1993). The failure of the algorithm to adequately remove the biased data is due, in part, to the difficulty in determining the optimal EIR threshold for all circumstances encountered in a given deployment, and to the presence, at times, of fish in all four beams at once.

4. ADCP Data Correction Methodology

A method for removing the fish bias utilizing MCM data has been developed by computing empirical orthogonal functions (EOFs) of demeaned ADCP–MCM speed differences at the depths of the MCMs. The first three eigenmodes for each deployment are shown in Figures 6–17. For the mean speed differences (Figures 18–29) and each eigenmode, a spline fit was performed on the differences at the MCM depths to create values at all intervening ADCP depths. The fish bias appeared negligible below 200 m, based on the weak variability observed in ADCP–MCM differences and EIR at 200–250 m. For this reason, and because the VACMs at 200 m and 250 m

may tend to overspeed by a few cm s^{-1} (Halpern, 1987), we forced the spline fits for both the mean differences and individual eigenvectors to zero at 200 m.

Only the first three eigenmodes were used in this correction scheme, because higher modes tended to be noisy. Also, we expect that not all of the differences between the ADCP and the MCM speeds were due to the presence of fish, and that the higher modes were capturing more subtle forms of instrument error in the MCMs and/or the ADCPs. Table 3 lists the percent variance corrected for each of the first three vertical modes for each deployment. For most deployments, 90% to 97% of the variance was explained by these three modes. For deployments only minimally affected by fish as indicated in both the EIR values and speed differences in Figures 4 and 5, percent variance explained by the first three EOFs was lower, e.g., 83.1% for PR01 and 84.5% for PR12. For each deployment, the means and first three vertical modes were combined to produce a correction file for the daily ADCP speeds at the ADCP depths. When the corrected ADCP speeds were compared with the MCM speeds there was considerable reduction in the standard deviation of the speed differences for each deployment (Figures 18–29).

In some of the mean speed difference plots (e.g., Figures 21, 24, 25, 28, and 29), the deployment-length mean ADCP–MCM difference goes from negative to positive at the depth of the Undercurrent core. This feature is even more pronounced during the first 2 weeks of each deployment where the fish bias errors are usually minimal. This mean difference pattern suggests that the ADCP velocities were actually from depths shallower than reported. To examine this hypothesis in greater detail, an RMS speed difference between the ADCP and MCM data was computed for each deployment using the first 2 weeks of data. The extrapolated 10-m ADCP depth and the 200-m depth with possible MCM overspeeding were not used in the calculation. The ADCP data were then remapped to shallower depths in 1-m increments and the RMS speed difference

Table 3. Percent variance corrected for each of the first 3 vertical modes and their total for each deployment.

140°W:	PR01	PR02	PR03	PR05	PR07	PR09	PR11	PR11A
Mode 1	49.2	62.7	43.5	47.8	83.8	56.7	77.8	73.3
Mode 2	18.3	18.7	34.4	30.7	7.9	21.6	12.3	14.7
Mode 3	15.6	11.8	12.6	11.8	4.7	11.7	5.8	7.2
Total	**83.1**	**93.2**	**90.5**	**90.3**	**96.4**	**90.0**	**95.9**	**95.2**

110°W:	PR04	PR06	PR08	PR12
Mode 1	81.9	61.4	89.0	49.0
Mode 2	11.8	21.2	4.4	20.8
Mode 3	3.4	7.2	4.1	14.7
Total	**97.1**	**89.8**	**97.5**	**84.5**

recomputed. Plots of RMS difference versus depth offset are shown in Figures 30a and 30b. The depth offsets associated with the minimum RMS speed difference indicate possible depth errors of 3–8 m for early deployments with the narrow bandwith tracking filter, and 1–4 m depth errors for later deployments with the broad bandwidth tracking filter to a depth below the Undercurrent core. Some of the apparent depth error in the early deployments may have been due to measurement skew. In addition to the bin 1 skew errors described in Pullen *et al.* (1992), RDI ADCP data with narrow bandwidth tracking filters and default time constants can have skew errors as large as several cm s^{-1} for much of the depth range in high shear zones (Lien *et al.*, 1994; Chereskin and Harding, 1993). Instrument tilt will also result in an average measurement depth which is less than the bin depth recorded (Pulkkinen, 1993). The EOF method corrects for skew- and tilt-related depth errors as well as for fish bias errors.

Before the corrected ADCP speeds were converted to zonal and meridional velocities, the differences between the ADCP and MCM directions were investigated. The ADCP–MCM direction differences (Figures 18–29) were computed such that the absolute value of the difference never exceeded 180 degrees. In many deployments, large standard deviations were evident in the upper 50 m. This shallow water variability was due, in part, to the presence of equatorial long waves (Pullen *et al.*, 1987). Data from a few of the MCMs were corrected for direction due to obvious calibration errors. Even so, mean ADCP–MCM direction differences were at times rather large, as great as 10° at 45 m in PR02, for example. One ADCP deployment, PR03, required a 6-degree rotation determined by comparison with 1.5 months of coincident ADCP data from a subsurface mooring deployed 13 km away as part of the Tropical Instability Wave Experiment (Weisberg *et al.*, 1991). In five of the deployments, the ADCP–MCM mean direction differences were positive for all the MCM depths, suggesting a mean error in the ADCP or the MCM calibration standard. Clearly, the accuracy of current velocity components is limited by uncertainties in compass direction measurements.

The ADCP directions did not appear affected by the presence of fish. Thus, corrected ADCP speeds and ADCP directions were used to compute daily profiles of zonal and meridional velocity at both mooring locations.

The data from the PR10 deployment at 110°W (from 6 November 1992 to 7 May 1993) were not corrected using the EOF analysis, since there were not sufficient MCM data at shallow depths to allow for the correction. However, as indicated by the EIR values in Figure 4, the data did not appear significantly affected by fish until the last month of the deployment. Thus, the daily averaged ADCP data from 6 November 1992 to 6 April 1993 were incorporated into the ADCP data base. Since the EOF analysis could not be applied, some depth and/or skew error may exist in the PR10 data. However, for this deployment, measured shear did not exceed .041 s^{-1}, and skew was minimized by use of the broad bandwidth low pass filter. There also did not appear to be any periods of extreme winds or currents that would possibly induce large instrument tilt.

Hourly EIR data from the last month of the PR10 deployment (7 April to 7 May 1993) indicated that, while the fish were present throughout the day in the upper 55 m, they were likely to be present only a portion of the day at greater depths. Thus, below 55 m, daily averages were computed using ADCP data from that part of the day when fish were not present as indicated by the EIR values (typically 2000 to 0200 local time). Above 55 m, the presence of fish throughout the day precluded using a similar technique to fill the gaps which remain in the final time series.

The ADCP data from 13–25 April 1993 at 140°W were not corrected using the EOF correction scheme, due to early failure of five of the MCMs at the end of the PR09 deployment. Hourly EIR data indicated a diurnal pattern to the presence of fish below 80 m, so daily averages at these depths were computed using ADCP data from the portion of the day that was minimally affected by fish (2000 to 0100 local time). The data from 13–25 April 1993 above 80 m could not be used.

5. Discussion

The first PROTEUS ADCP, PR01 at 140°W, was deployed in May 1990 on a mooring with no MCMs in the mooring line. MCMs, however, were deployed on a separate mooring 16 km away. As mentioned earlier, the PR01 ADCP data apparently were not significantly affected by the presence of fish. Beginning in October 1990, the standard deployment configuration contained both the ADCP and the MCMs on the same mooring. To test whether the addition of MCMs to the ADCP mooring line was causing the fish bias problem by attracting fish to the mooring for whatever reason, two moorings were deployed at 140°W in April 1993. PR11a was deployed with no MCMs in the mooring line and PR11 was deployed 15 km away in the standard ADCP–MCM configuration. As shown in Figure 5b, both deployments exhibited large fish bias errors. The errors in the PR11a data were somewhat smaller, probably due to the fact that the ADCP on PR11a was equipped with a fish rejection algorithm, whereas that on PR11 was not. The errors began somewhat earlier in the record at the same depth for PR11. This could be interpreted to suggest that fish were more readily attracted to PR11 with the MCMs in the mooring line, although it is equally plausible that earlier development of biases on PR11 was due strictly to chance.

Although the removal of the MCMs from the mooring line did not eliminate large fish bias errors, the nearby ADCP deployments provided an opportunity to test the consistency of the EOF correction method. For comparison of the two deployments, contour plots of the echo intensity range are shown in Figure 31. Both plots show an increase in echo intensity range beginning in late June 1993, with significant values extending from the surface to 100 m by September. The presence of fish is clearly more evident in the PR11 deployment, as evidenced by the greater magnitude and temporal extent of the PR11 EIR values.

As would be expected, the EOF eigenvectors and time series were different for the PR11 and PR11a deployments (Figures 15 and 16), particularly in early August when the evidence of fish was much stronger in PR11. The ADCP speed corrections derived from the EOF analysis for both

deployments show these differences clearly (Figure 32). To evaluate the consistency of the EOF analysis, the corrected speeds from the two deployments were differenced (Figure 33). These differences were generally small, with extreme values for any depth bin ranging from –13 to 16 cm s^{-1}. The deployment length mean differences for any depth bin were less than ±1 cm s^{-1}, with difference standard deviations less than 5 cm s^{-1}. These differences are within instrument accuracies and ocean variability over 15 km and provide confidence in the analysis techniques.

Contour plots of the full corrected data for 1991–1993 at 110°W and 1990–1993 at 140°W are shown in Figures 34 and 35. Data gaps occur in boreal spring 1993 in the upper 55 m for 1 month at 110°W and in the upper 80 m for 2 weeks at 140°W. As discusssed earlier, the time series at these times could not be EOF-corrected due to the lack of available MCM data.

6. Conclusions

Large speed errors were evident in the ADCP data from equatorial moorings at 110°W and 140°W due to the reflection of acoustic energy from pelagic fish attracted to the vicinity of the moorings. A method was developed for removing the bias based on an EOF analysis of ADCP–MCM speed differences. The corrected speeds were combined with the ADCP directions to produce daily profiles of zonal and meridional velocity. The corrected ADCP velocity profiles provide a significantly improved data set, with finer vertical resolution and fewer data gaps than the MCM data, and greater accuracy than the uncorrected ADCP data.

7. Acknowledgments

We would like to thank Professor Robert Weisberg (University of South Florida) for providing upward-looking ADCP data from 0°, 140°W. This work was supported by NOAA's U.S. TOGA Project Office and the Equatorial Pacific Ocean Climate Studies (EPOCS) program.

8. References

Anonymous, 1989: *Acoustic Doppler current profilers, principles of operation: a practical primer*, R.D. Instruments, 36 pp.

Beardsley, R.C., 1987: A comparison of the vector-averaging current meter and New Edgerton, Germeshausen, and Grier, Inc., vector-measuring current meter on a surface mooring in Coastal Dynamics Experiment 1. *J. Geophys. Res., 92*, 1845–1859.

Chereskin, T.K., and A.J. Harding, 1993: Modelling the performance of an acoustic Doppler current profiler. *J. Atmos. Ocean. Tech., 10*, 41–63.

Freitag, H.P., M.J. McPhaden, and P.E. Pullen, 1992: Fish-induced bias in acoustic Doppler current profiler data. *Proceedings, Oceans '92, Mastering the Oceans Through Technology*, October 26–29, 1992, Newport, RI, 712–717.

Freitag, H.P., P.E. Plimpton, and M.J. McPhaden, 1993: Evaluation of an ADCP fish-bias rejection algorithm. *Proceedings, Oceans '93, Engineering in Harmony with the Ocean*, Vol. II, October 18–21, 1993, Victoria, Canada, 394–397.

Halpern, D., 1987: Comparison of upper ocean VACM and VMCM observations in the equatorial Pacific. *J. Atmos. Ocean. Tech., 4*, 84–93.

Hayes, S.P., L.J. Mangum, J. Picaut, A. Sumi, and K. Takeuchi, 1991: TOGA-TAO: A moored array for real-time measurements in the tropical Pacific Ocean. *Bull. Am. Meteorol. Soc., 72*, 339–347.

Karweit, M., 1974: Response of a Savonious rotor to unsteady flow. *J. Mar. Res., 32*, 359–364.

Lien, R. C., M. J. McPhaden, and D. Hebert, 1994: Intercomparison of ADCP measurements at 0°, 140°W. *J. Atmos. Ocean. Tech., 11*, 1334–1339.

McPhaden, M.J., 1993: TOGA-TAO and the 1991–1993 El Niño-Southern Oscillation Event. *Oceanography, 6*, 36-44.

McPhaden, M.J., H.B. Milburn, A.I. Nakamura, and A.J. Shepherd, 1990: PROTEUS–Profile telemetry of upper ocean currents. *Proceedings of the MTS '90 Conference*, September 26–28, Marine Technology Society, Washington, D.C., 353–357.

Pulkkinen, K., 1993: Comparison of different bin-mapping methods for a bottom-mounted acoustic profiler. *J. Atmos. Ocean. Tech., 10*, 404–409.

Pullen, P.E., M.J. McPhaden, H.P. Freitag, and J. Gast, 1992: Surface wave induced skew errors in acoustic Doppler current profiler measurements from high shear regimes. *Proceedings, Oceans '92, Mastering the Oceans Through Technology*, October 26–29, 1992, Newport, RI, 706–711.

Pullen, P.E., R.L. Bernstein, and D. Halpern, 1987: Equatorial long-wave characteristics determined from satellite sea surface temperature and in situ data. *J. Geophys. Res., 92*(C1), 742–748.

Weisberg, R.H., J.C. Donovan, and R.D. Cole, 1991: The tropical instability wave experiment (TIWE) equatorial array. Univ. of S. Florida Data Report, St. Petersburg, FL, 84 pp.

Weller, R.A., and R.E. Davis, 1980: A vector-measuring current meter. *Deep-Sea Res., 27*, 575–582.

Wilson, C.D., and E. Firing, 1992: Sunrise swimmers bias acoustic Doppler current profiles. *Deep-Sea Res., 39*, 885–892.

FIGURES

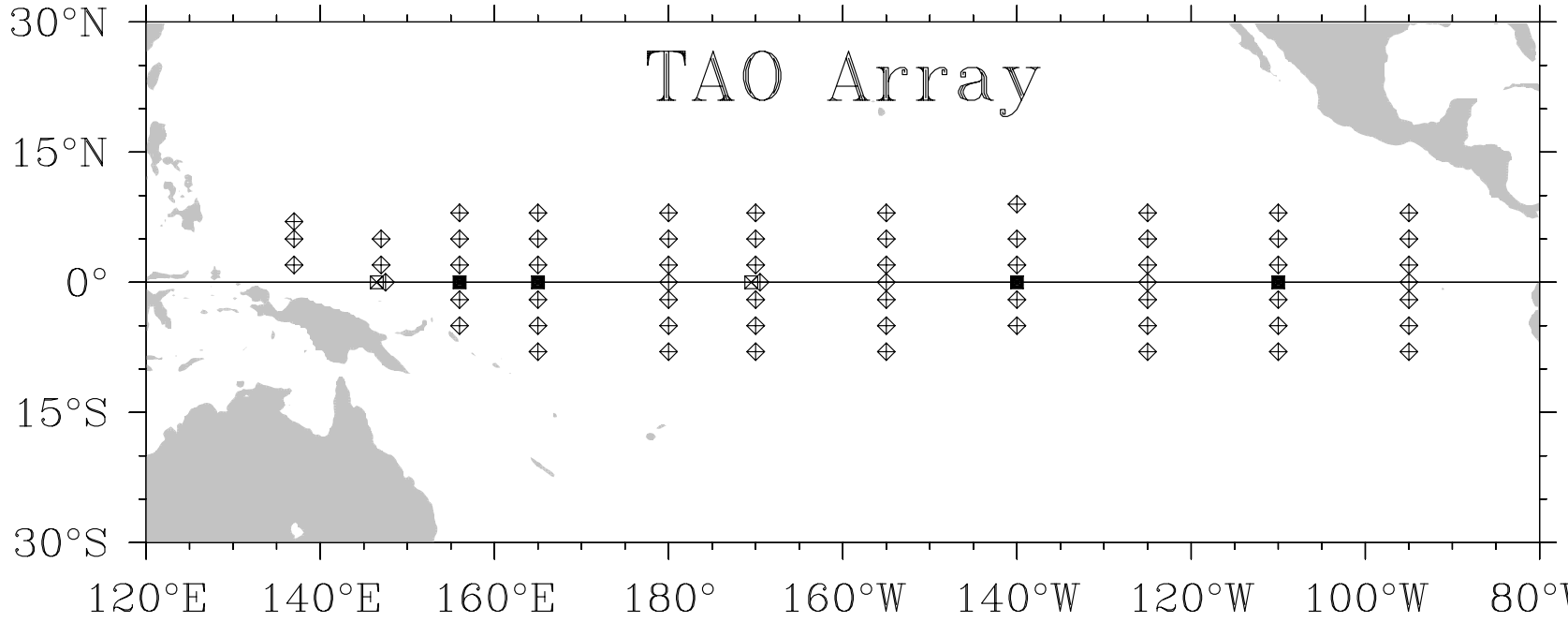

Fig. 1. Tropical Ocean Atmosphere (TAO) array of ATLAS wind and thermistor chain moorings (diamonds) and current meter moorings (squares). Solid squares indicate sites instrumented with telemetering PROTEUS current meter moorings.

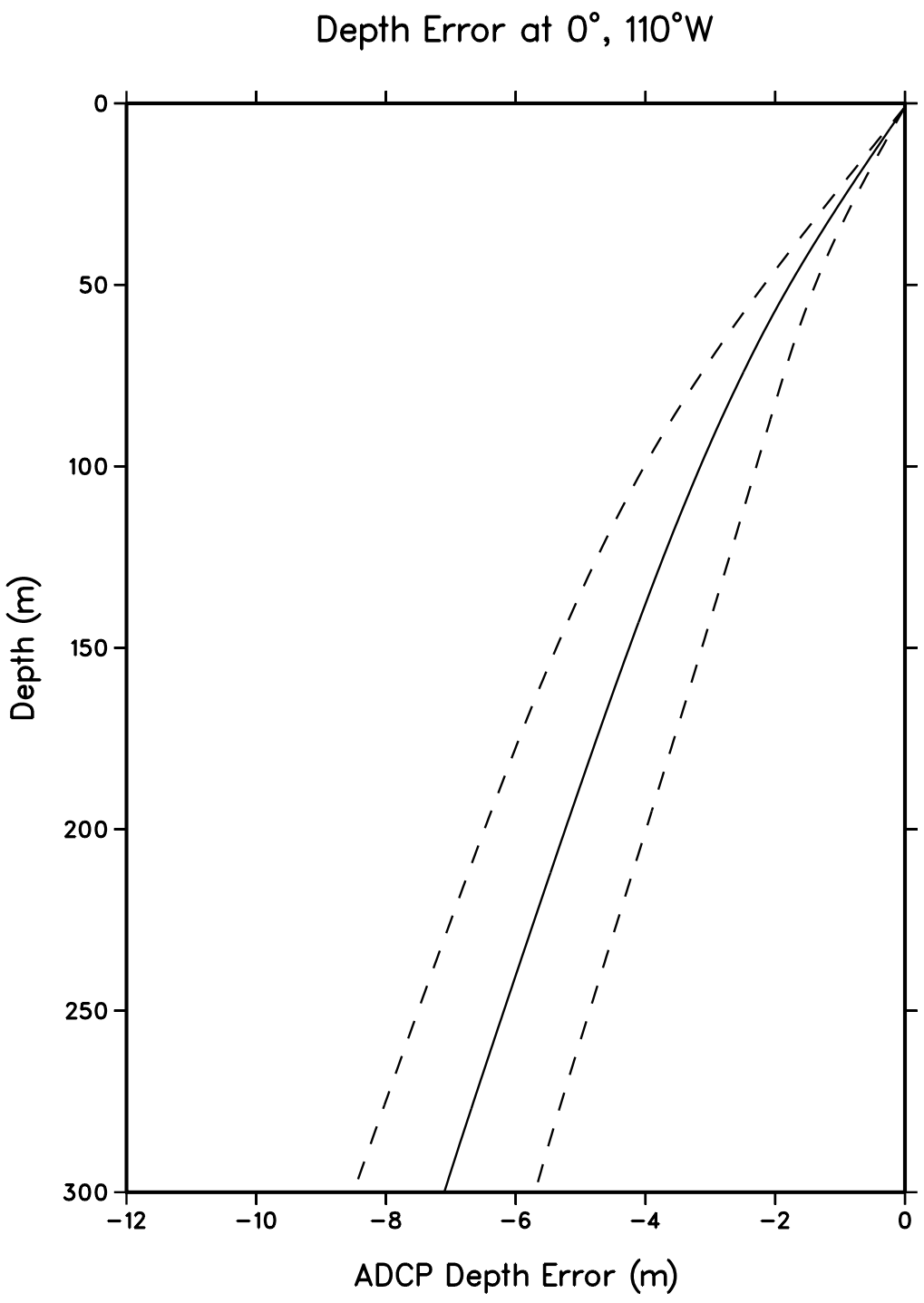

Fig. 2a. Depth error of nominal ADCP depth bin lengths which assume a constant sound speed with depth of 1475.1 m s^{-1}. Mean sound velocities and standard deviations versus depth were computed from historical hydrographic data at 0°, 110°W. The mean sound speed ±2 standard deviations was also used in the calculation to indicate the possible variations in depth error (dashed lines).

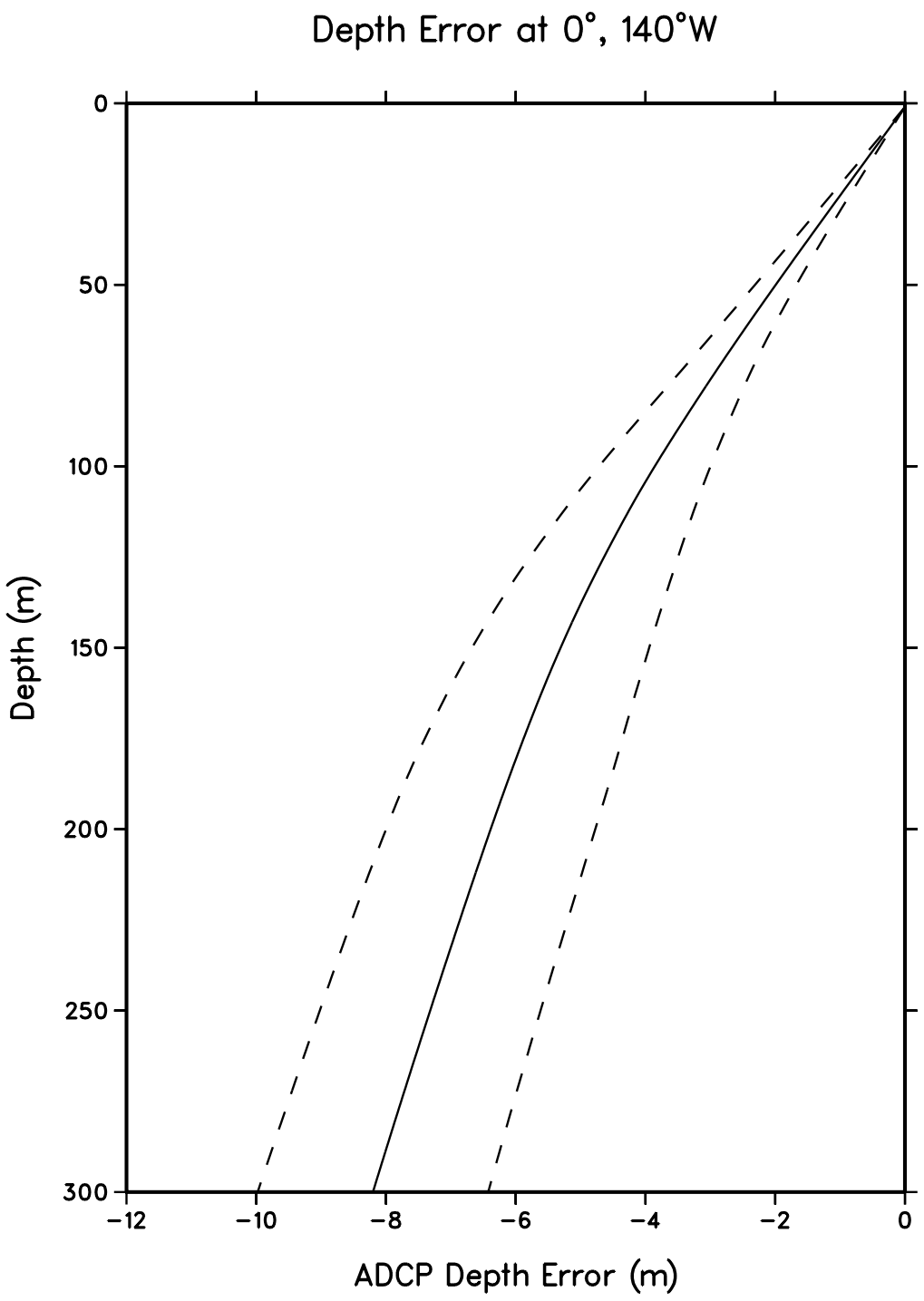

Fig. 2b. Depth error of nominal ADCP depth bin lengths which assume a constant sound speed with depth of 1475.1 m s^{-1}. Mean sound velocities and standard deviations versus depth were computed from historical hydrographic data at 0°, 140°W. The mean sound speed ±2 standard deviations was also used in the calculation to indicate the possible variations in depth error (dashed lines).

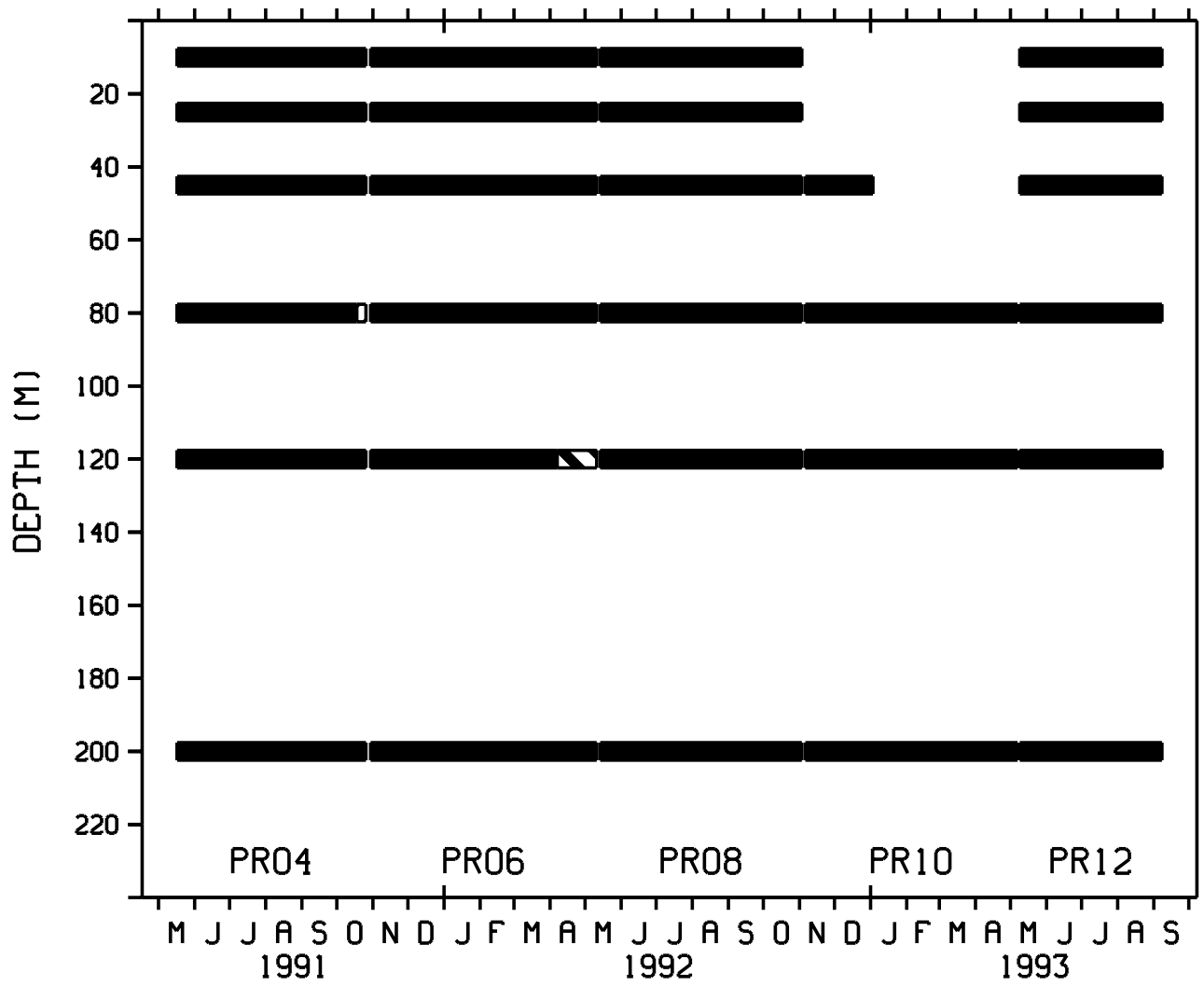

Fig. 3a. Depth and time coverage of mechanical current meter data at 0°, 110°W. Areas of thick striping are data filled using ADCP data from the portion of the day that was minimally affected by fish. Gaps at shallow depths of deployment PR10 (6 Nov 1992 to 7 May 1993) could not be filled.

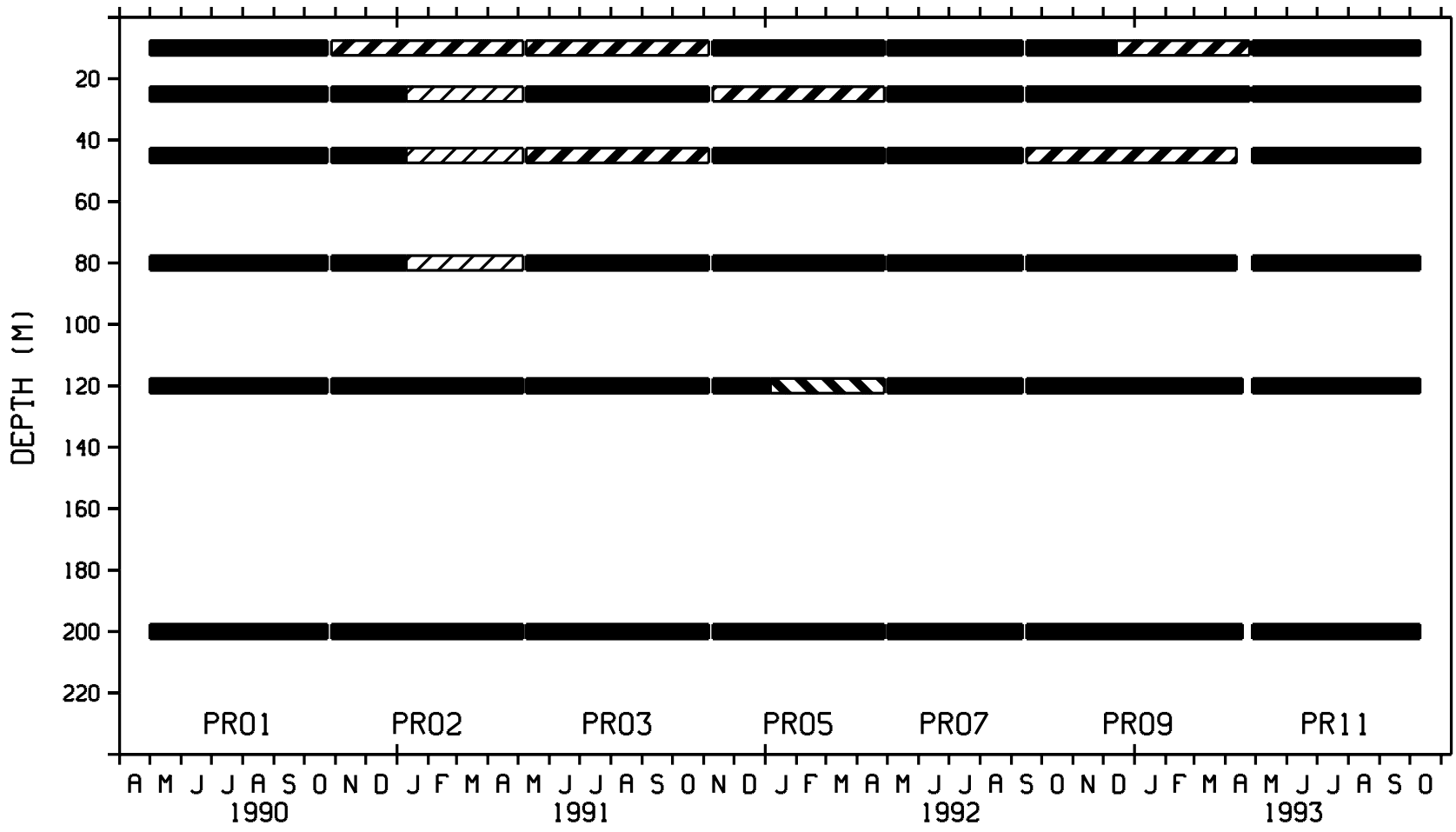

Fig. 3b. Depth and time coverage of mechanical current meter data at 0°, 140°W. Areas of thick striping at 10, 25, and 45 m are data filled using interpolation or linear regression techniques. Thick striping at 120 m indicates gaps filled using ADCP data from the portion of the day that was minimally affected by fish. Areas of thin striping are MCM data corrected for biofouling using data from an upward looking ADCP.

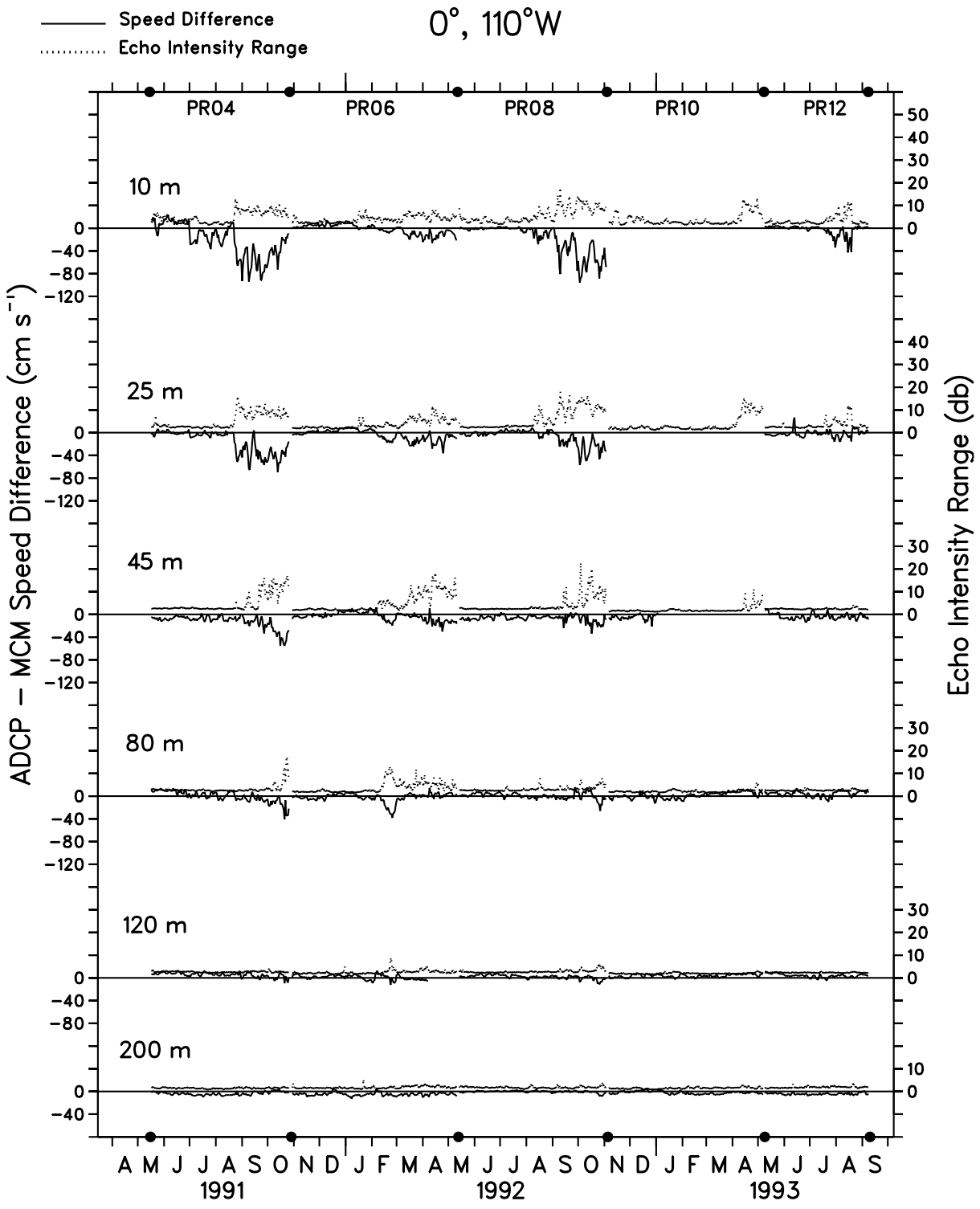

Fig. 4. Time series of ADCP–MCM speed difference and echo intensity range for five deployments at 0°, 110°W. Deployment and recovery times of the moorings are shown by black dots at the abscissas. At 10-m depth, the ADCP speed data have been linearly extrapolated from the bin 1 depth of 14 m for the comparison.

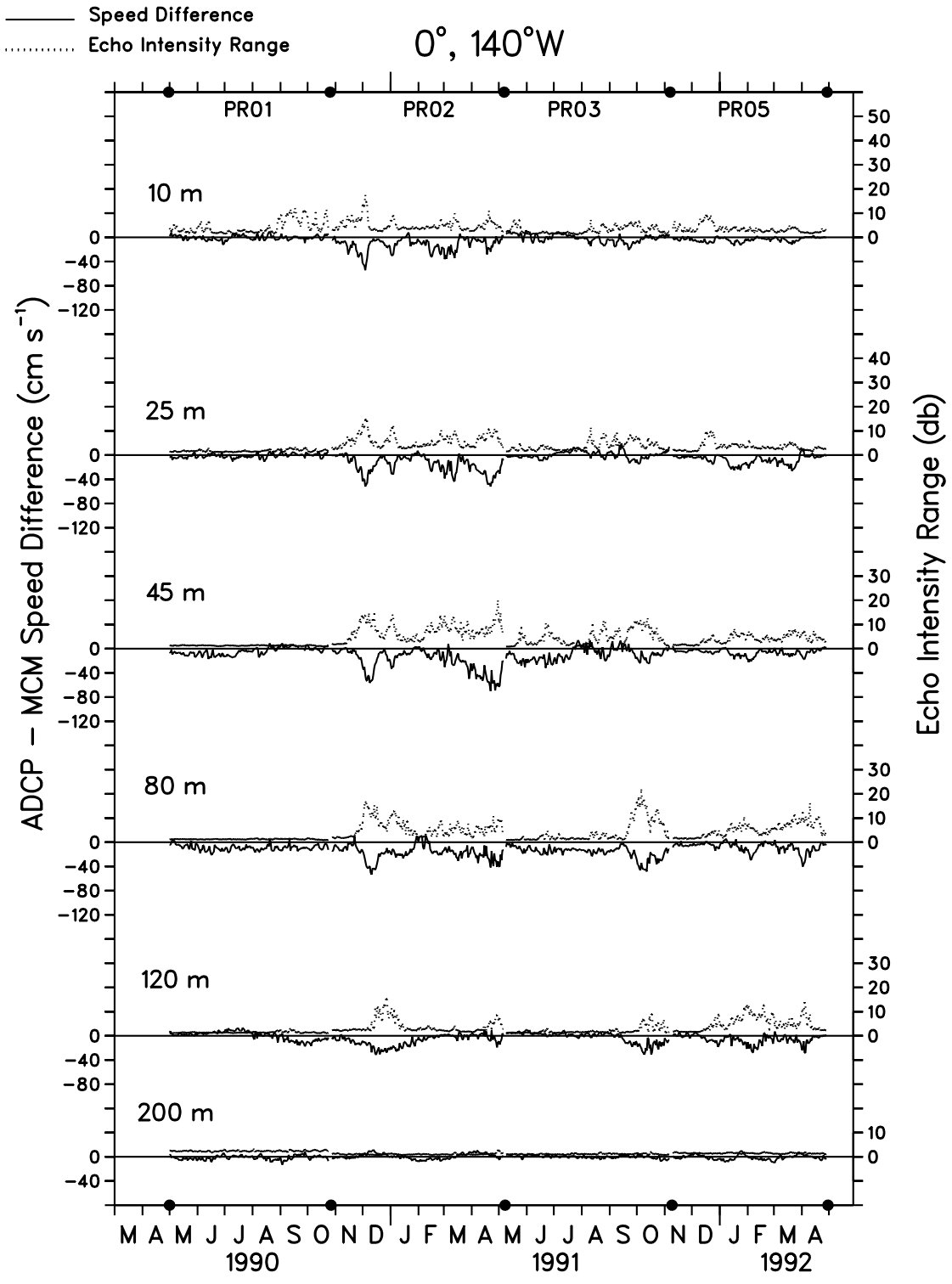

Fig. 5a. Time series of ADCP–MCM speed difference and echo intensity range for four deployments at 0°, 140°W. Deployment and recovery times of the moorings are shown by black dots at the abscissas. At 10-m depth, the ADCP speed data have been linearly extrapolated from the bin 1 depth of 14 m for the comparison.

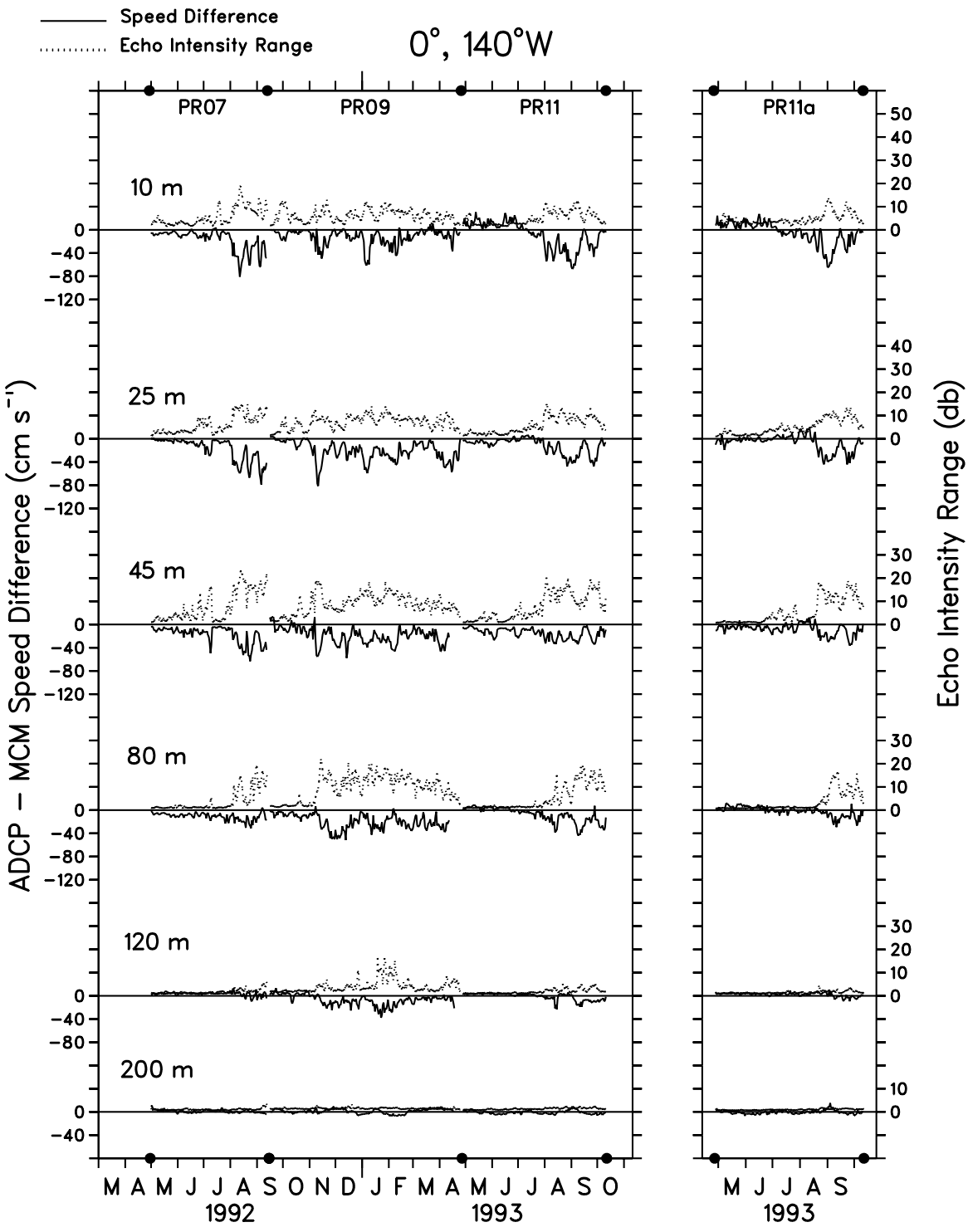

Fig. 5b. Time series of ADCP–MCM speed difference and echo intensity range for four ADCP and three MCM deployments at 0°, 140°W. Deployment and recovery times of the moorings are shown by black dots at the abscissas. To compute PR11a speed differences, ADCP speeds from PR11a are differenced with MCM speeds from PR11. At 10-m depth, the ADCP speed data have been linearly extrapolated from the bin 1 depth of 14 m for the comparison.

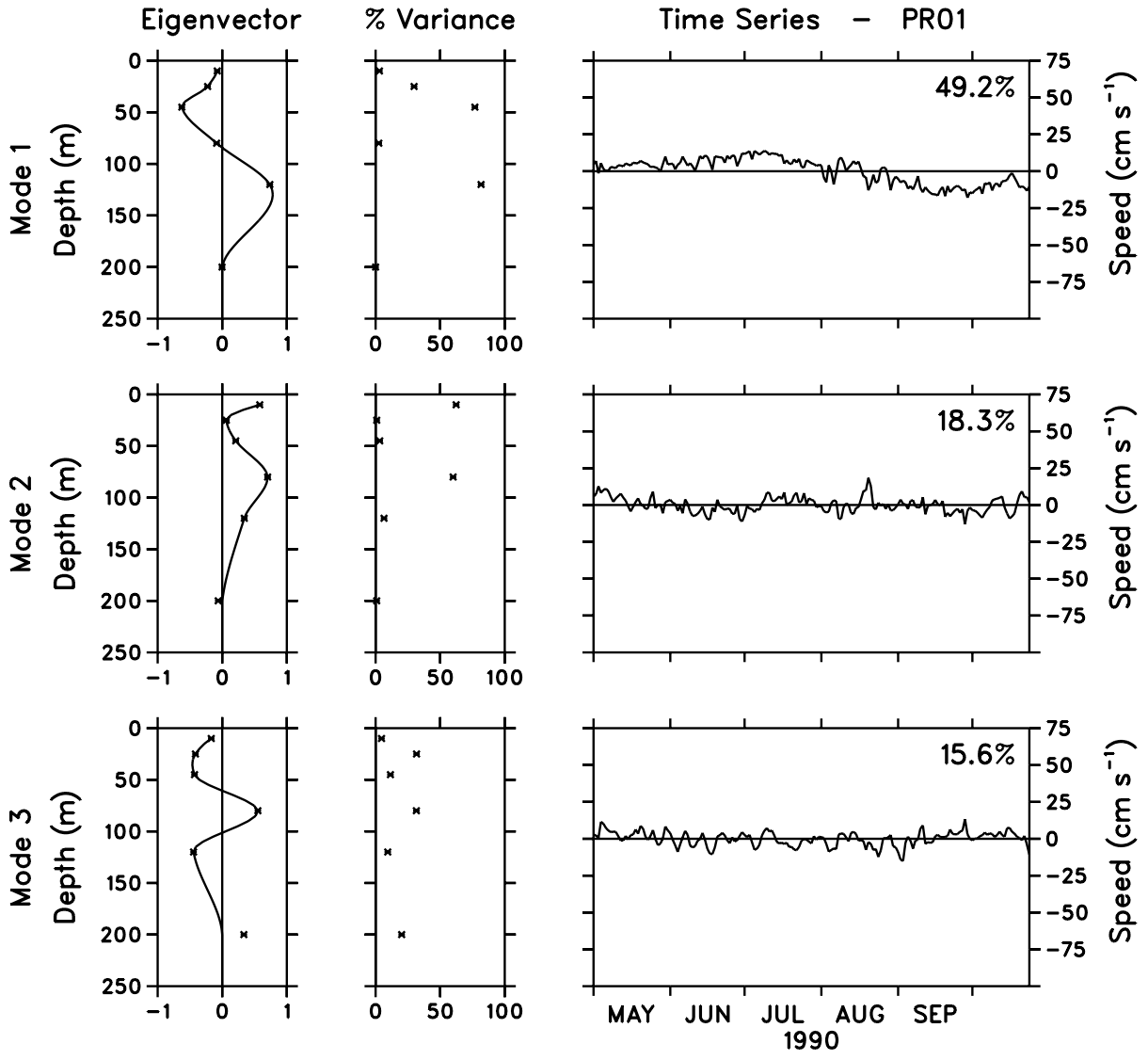

Fig. 6. The first three EOF eigenvectors and time series of ADCP–MCM speed differences for PR01. Percent variance explained at each depth is shown in the center panel. Percent of total variance explained by each EOF is shown in the upper right hand corner of the time series panel. The symbols (x) indicate values at individual MCM depths; the solid curve through the individual eigenvector values is a spline fit which has been forced to zero at 200 m.

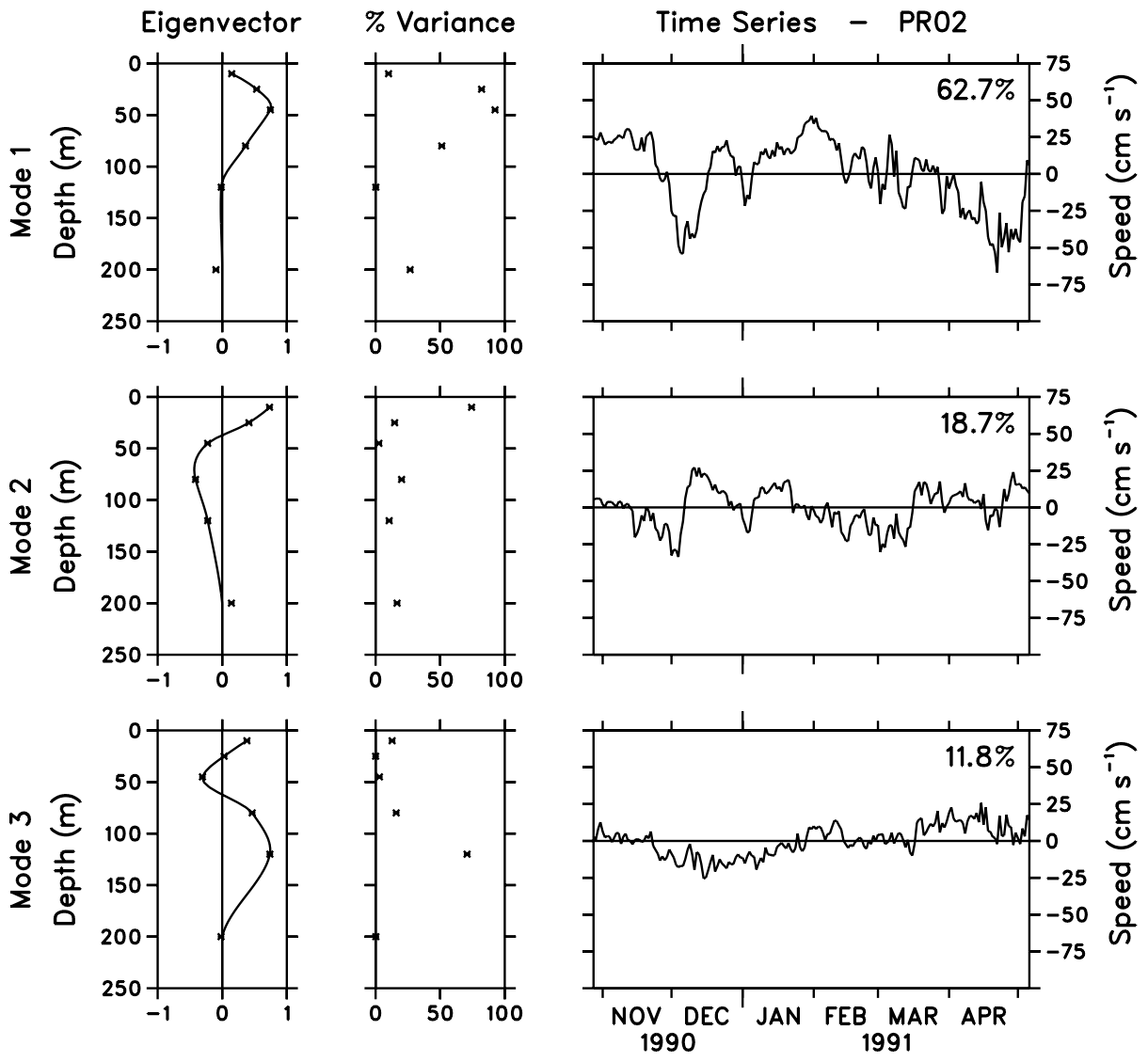

Fig. 7. The first three EOF eigenvectors and time series of ADCP–MCM speed differences for PR02. Percent variance explained at each depth is shown in the center panel. Percent of total variance explained by each EOF is shown in the upper right hand corner of the time series panel. The symbols (x) indicate values at individual MCM depths; the solid curve through the individual eigenvector values is a spline fit which has been forced to zero at 200 m.

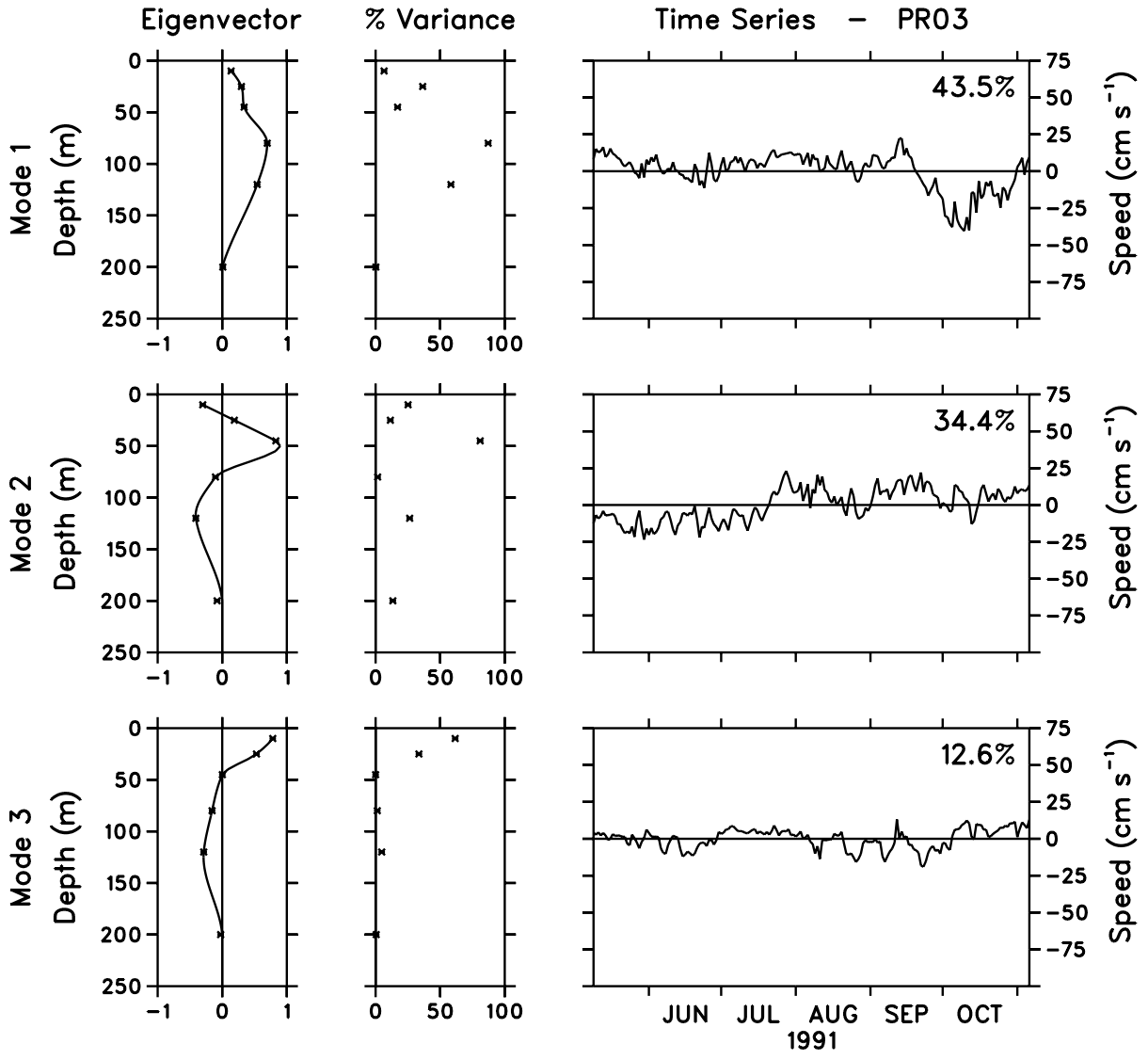

Fig. 8. The first three EOF eigenvectors and time series of ADCP–MCM speed differences for PR03. Percent variance explained at each depth is shown in the center panel. Percent of total variance explained by each EOF is shown in the upper right hand corner of the time series panel. The symbols (x) indicate values at individual MCM depths; the solid curve through the individual eigenvector values is a spline fit which has been forced to zero at 200 m.

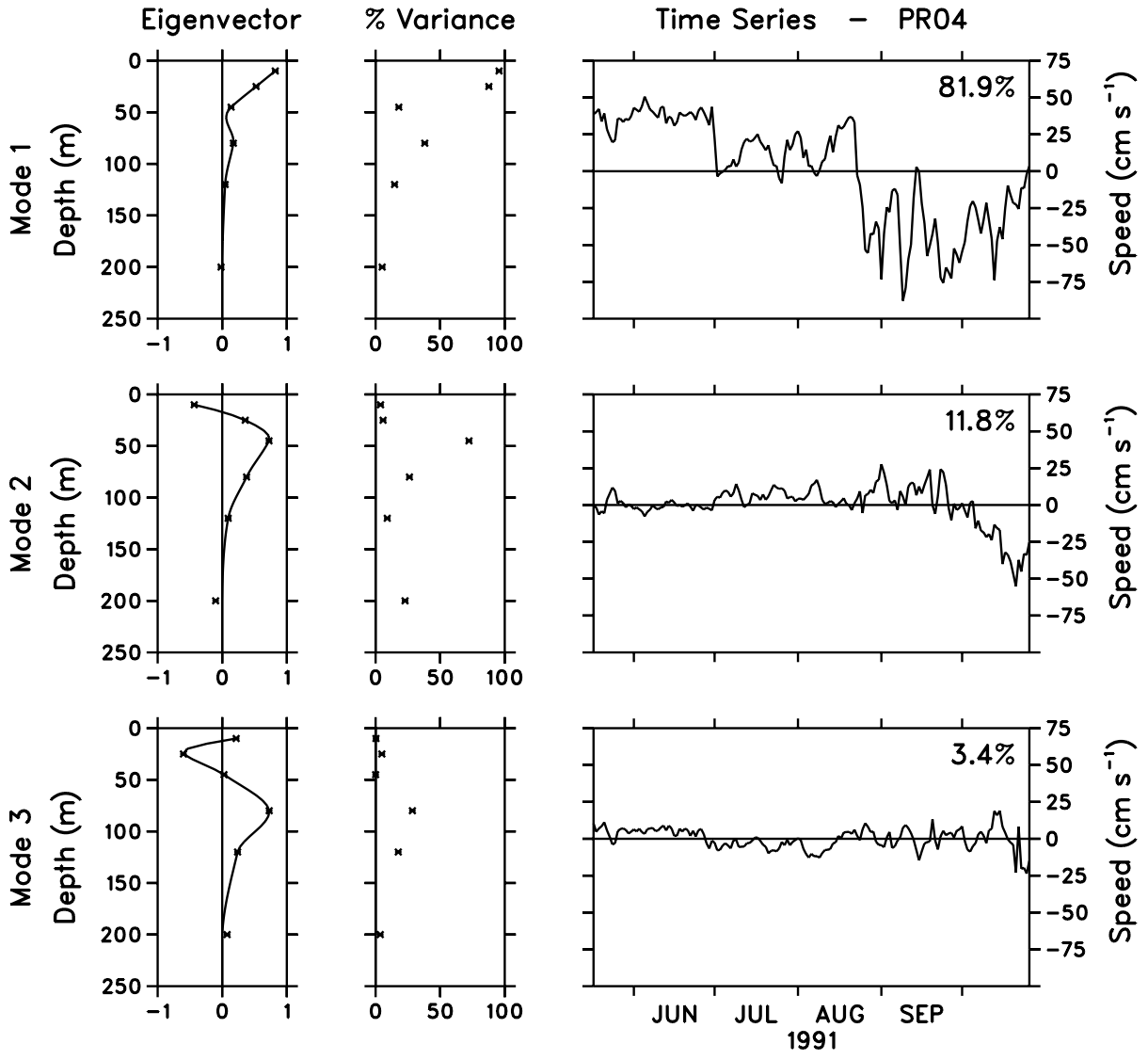

Fig. 9. The first three EOF eigenvectors and time series of ADCP–MCM speed differences for PR04. Percent variance explained at each depth is shown in the center panel. Percent of total variance explained by each EOF is shown in the upper right hand corner of the time series panel. The symbols (x) indicate values at individual MCM depths; the solid curve through the individual eigenvector values is a spline fit which has been forced to zero at 200 m.

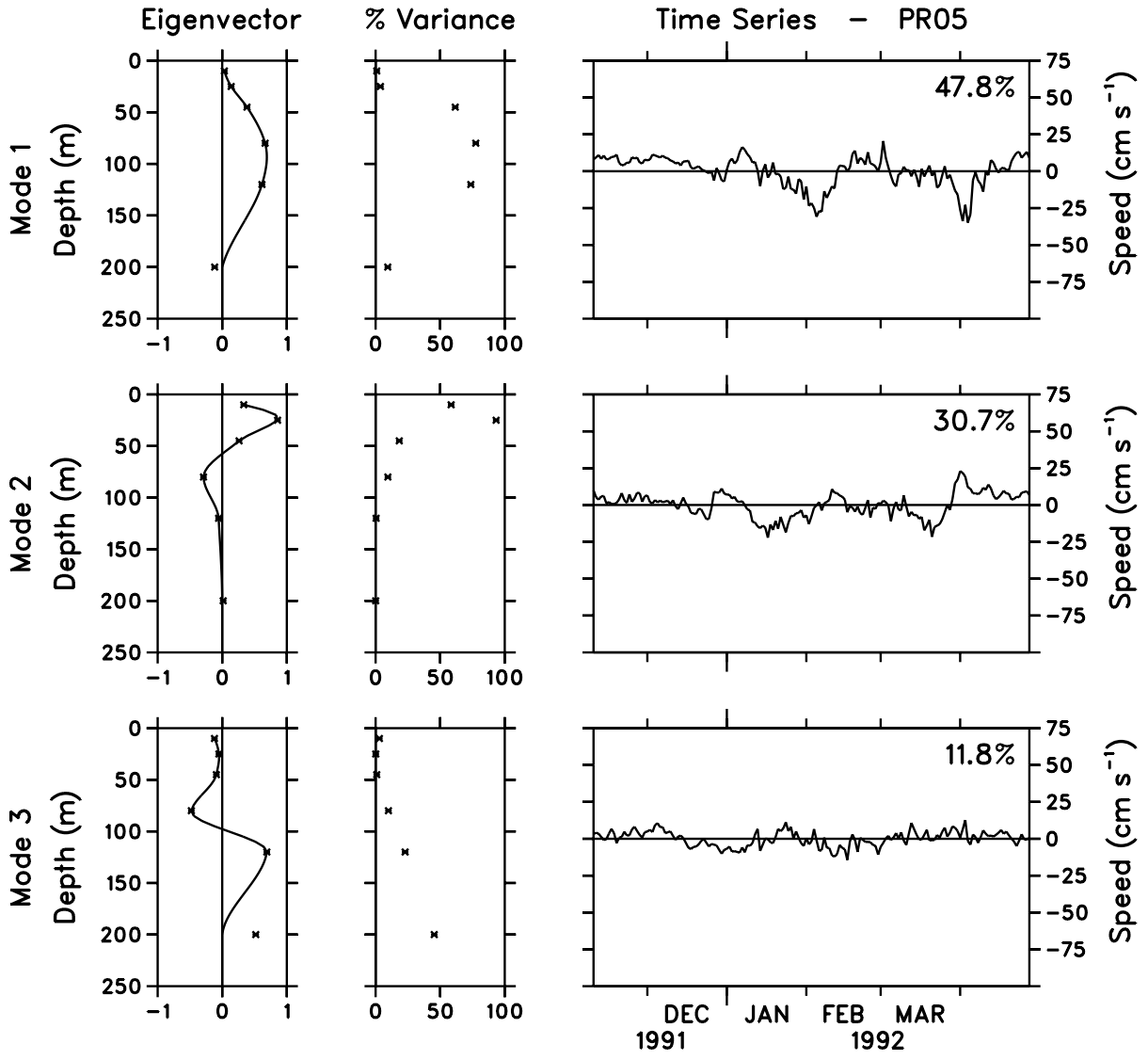

Fig. 10. The first three EOF eigenvectors and time series of ADCP–MCM speed differences for PR05. Percent variance explained at each depth is shown in the center panel. Percent of total variance explained by each EOF is shown in the upper right hand corner of the time series panel. The symbols (x) indicate values at individual MCM depths; the solid curve through the individual eigenvector values is a spline fit which has been forced to zero at 200 m.

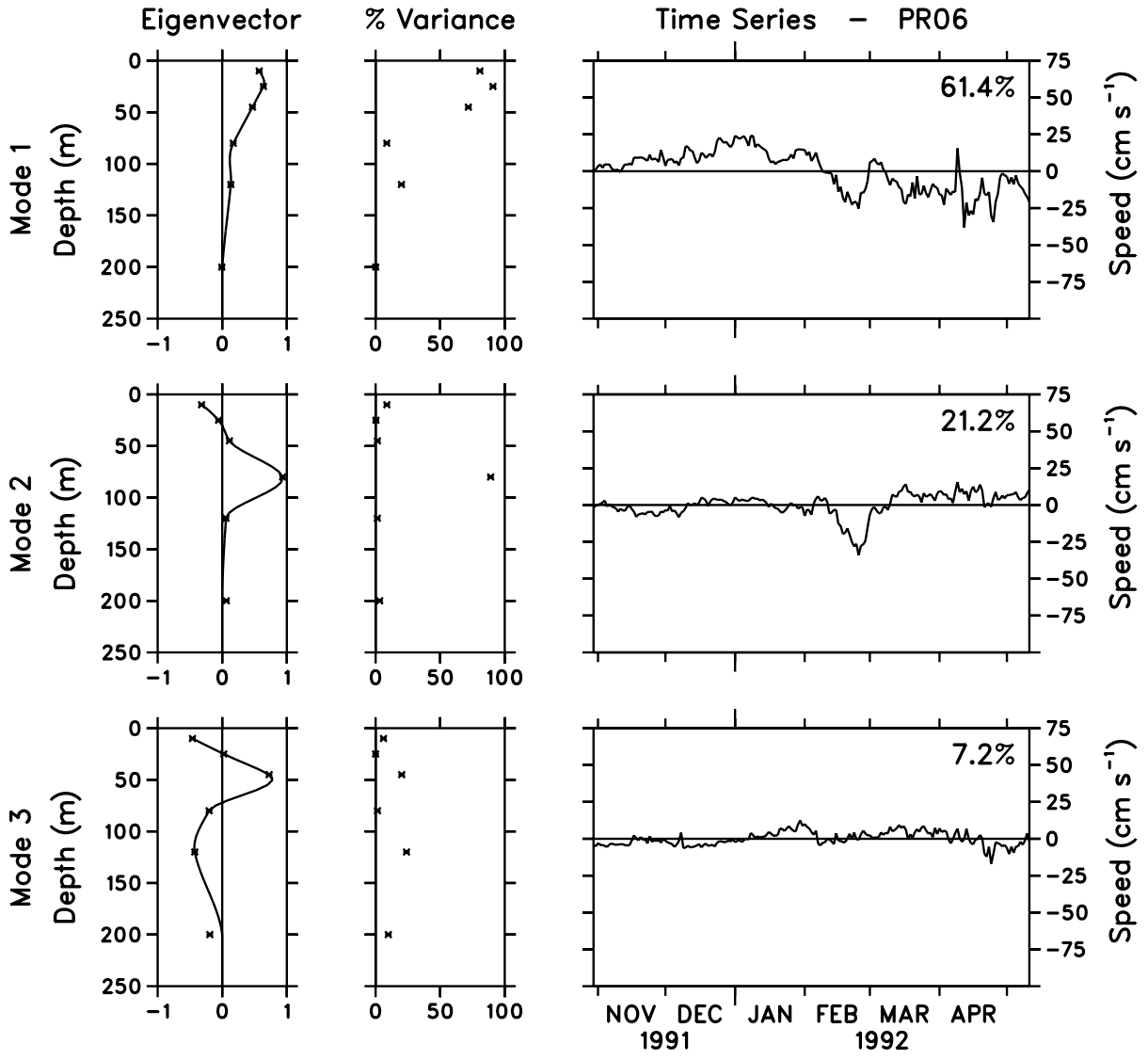

Fig. 11. The first three EOF eigenvectors and time series of ADCP–MCM speed differences for PR06. Percent variance explained at each depth is shown in the center panel. Percent of total variance explained by each EOF is shown in the upper right hand corner of the time series panel. The symbols (x) indicate values at individual MCM depths; the solid curve through the individual eigenvector values is a spline fit which has been forced to zero at 200 m.

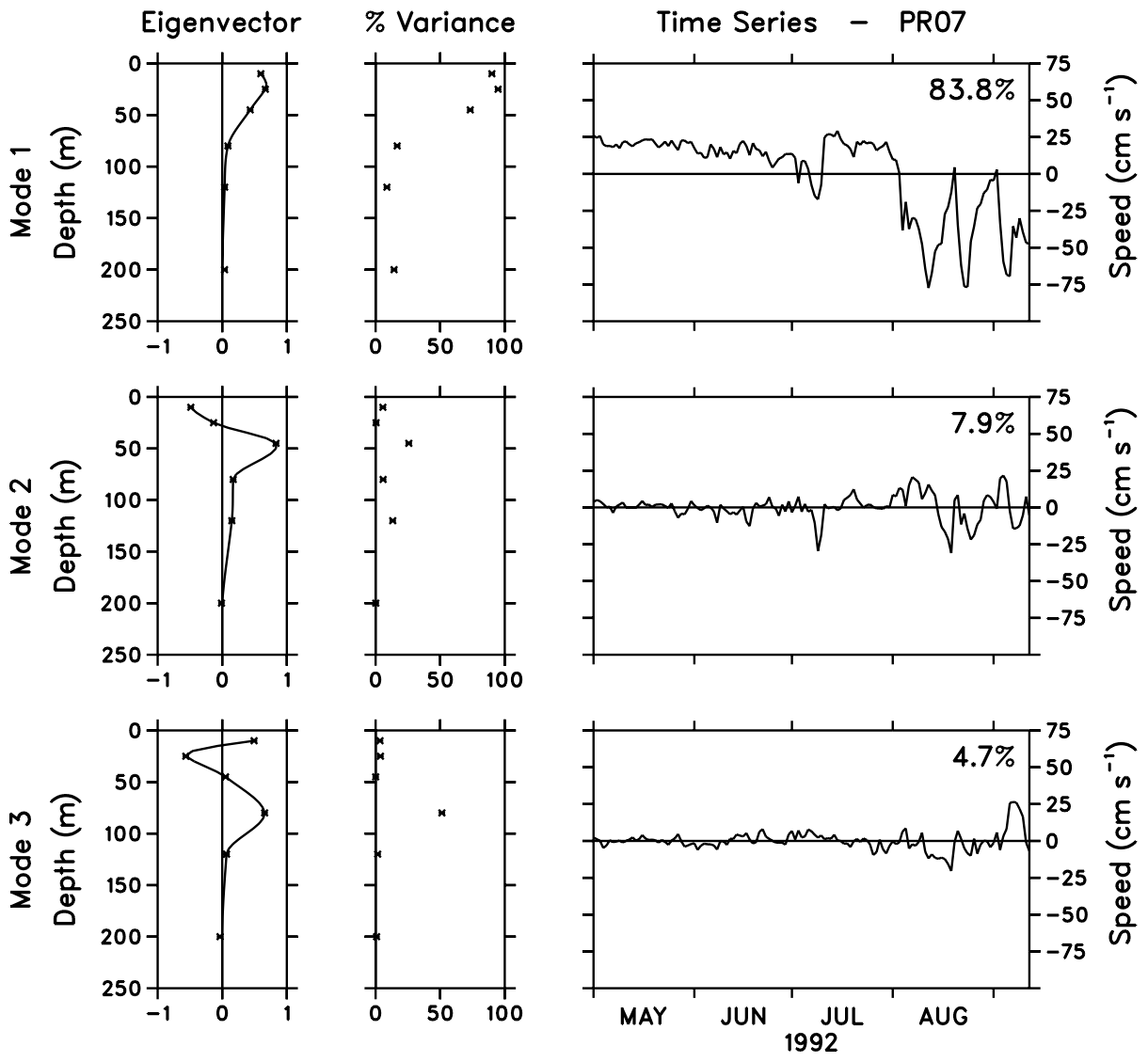

Fig. 12. The first three EOF eigenvectors and time series of ADCP–MCM speed differences for PR07. Percent variance explained at each depth is shown in the center panel. Percent of total variance explained by each EOF is shown in the upper right hand corner of the time series panel. The symbols (x) indicate values at individual MCM depths; the solid curve through the individual eigenvector values is a spline fit which has been forced to zero at 200 m.

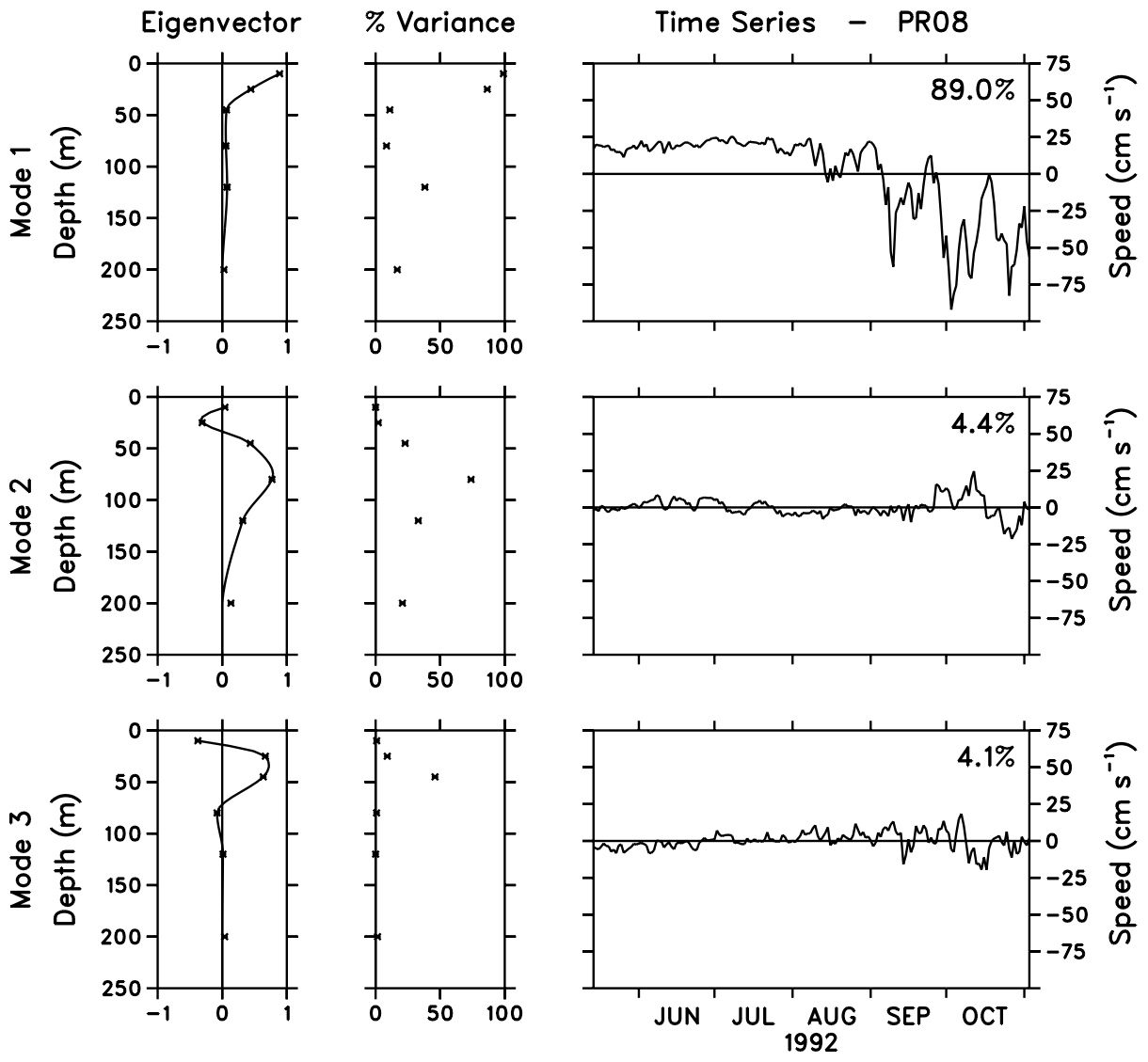

Fig. 13. The first three EOF eigenvectors and time series of ADCP–MCM speed differences for PR08. Percent variance explained at each depth is shown in the center panel. Percent of total variance explained by each EOF is shown in the upper right hand corner of the time series panel. The symbols (x) indicate values at individual MCM depths; the solid curve through the individual eigenvector values is a spline fit which has been forced to zero at 200 m.

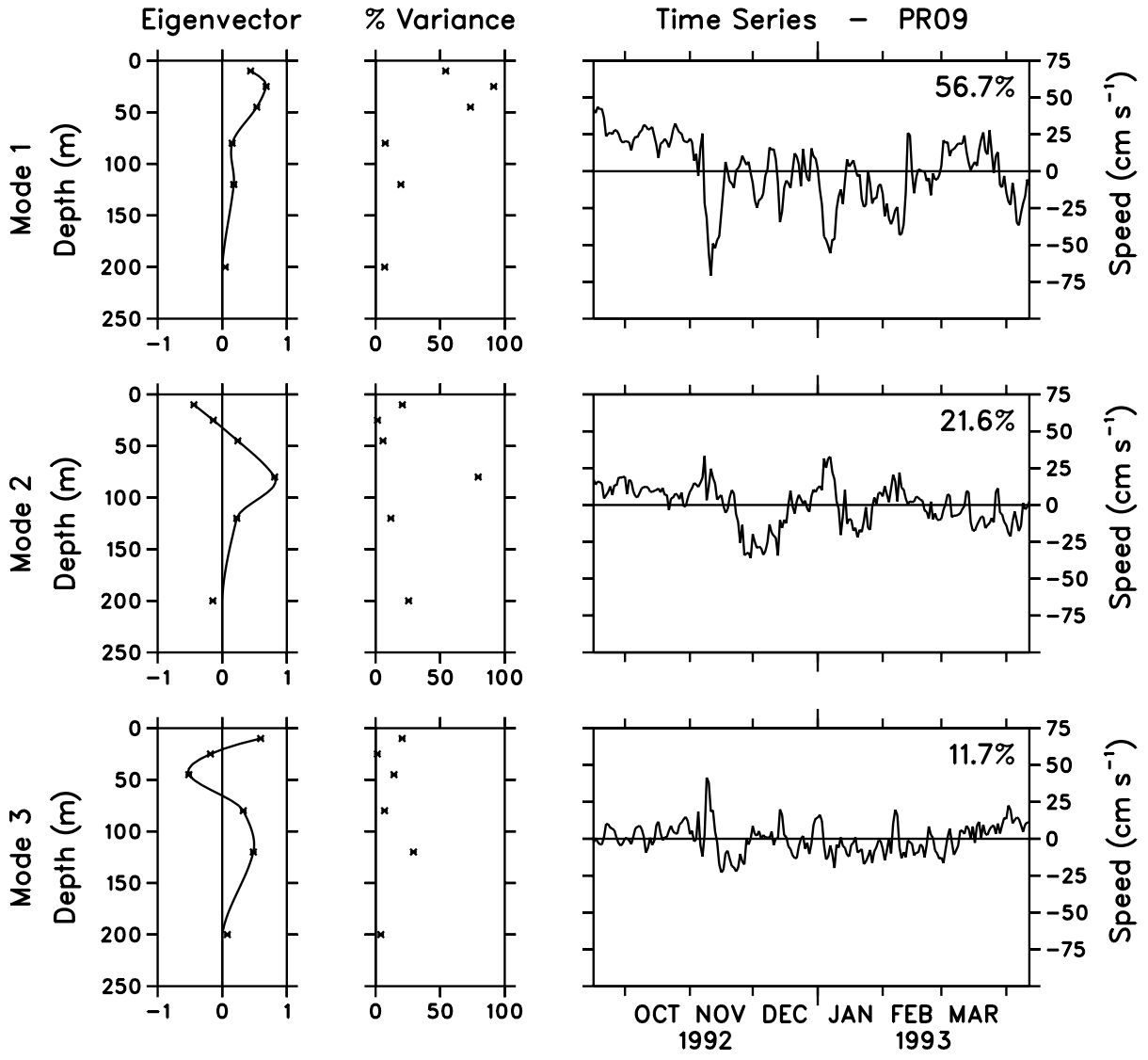

Fig. 14. The first three EOF eigenvectors and time series of ADCP–MCM speed differences for PR09. Percent variance explained at each depth is shown in the center panel. Percent of total variance explained by each EOF is shown in the upper right hand corner of the time series panel. The symbols (x) indicate values at individual MCM depths; the solid curve through the individual eigenvector values is a spline fit which has been forced to zero at 200 m.

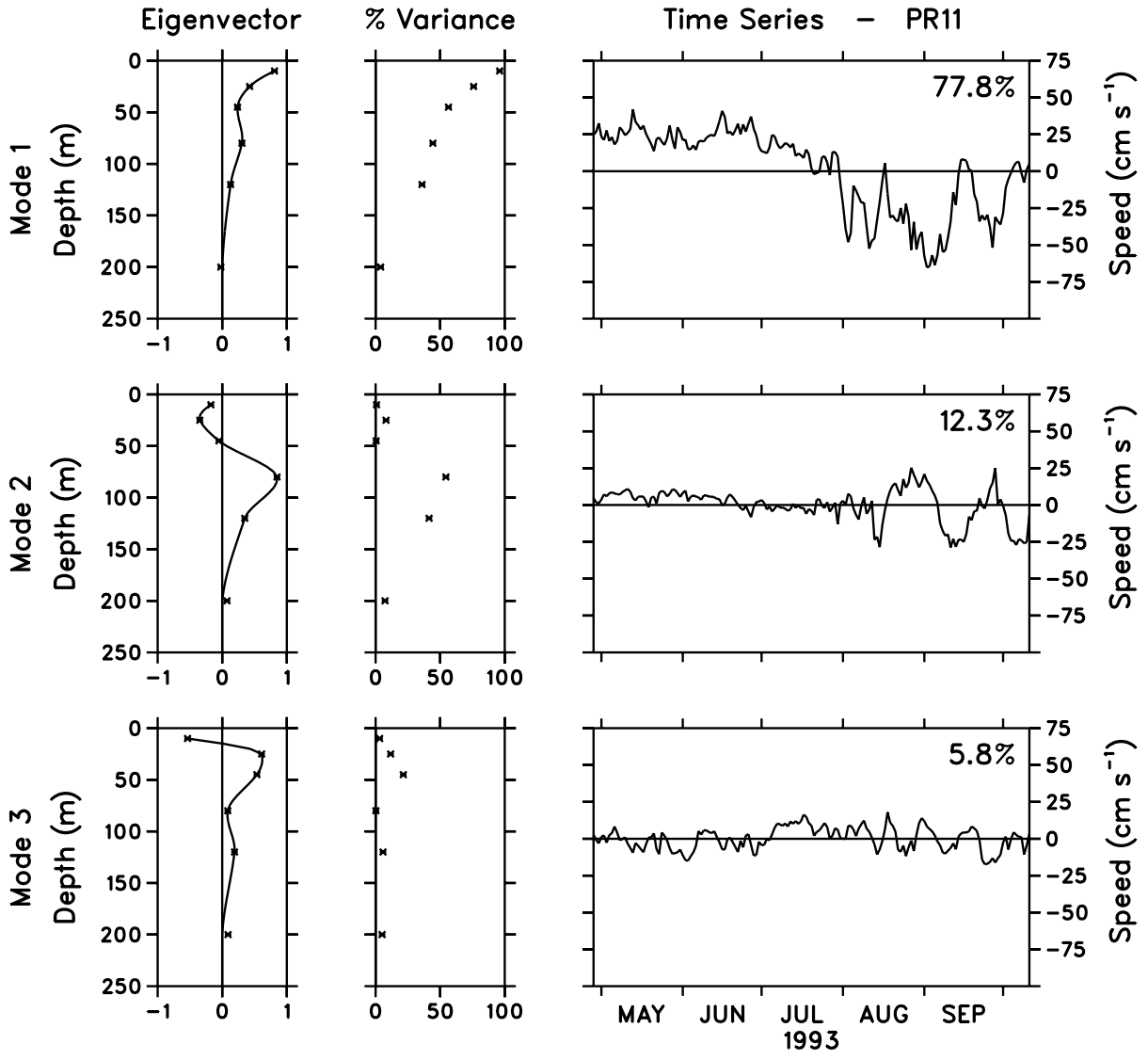

Fig. 15. The first three EOF eigenvectors and time series of ADCP–MCM speed differences for PR11. Percent variance explained at each depth is shown in the center panel. Percent of total variance explained by each EOF is shown in the upper right hand corner of the time series panel. The symbols (x) indicate values at individual MCM depths; the solid curve through the individual eigenvector values is a spline fit which has been forced to zero at 200 m.

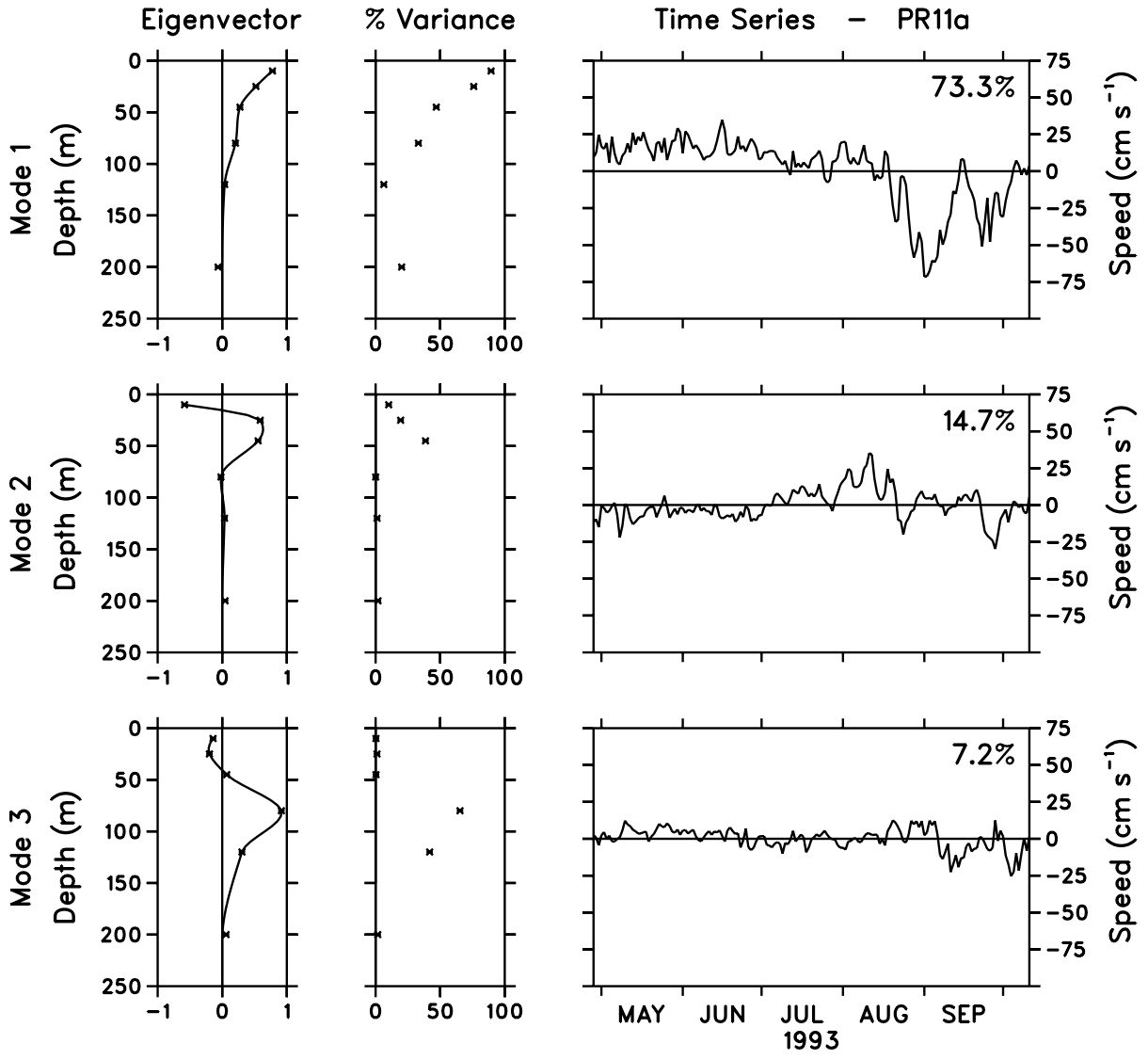

Fig. 16. The first three EOF eigenvectors and time series of ADCP–MCM speed differences for PR11a. Percent variance explained at each depth is shown in the center panel. Percent of total variance explained by each EOF is shown in the upper right hand corner of the time series panel. The symbols (x) indicate values at individual MCM depths; the solid curve through the individual eigenvector values is a spline fit which has been forced to zero at 200 m.

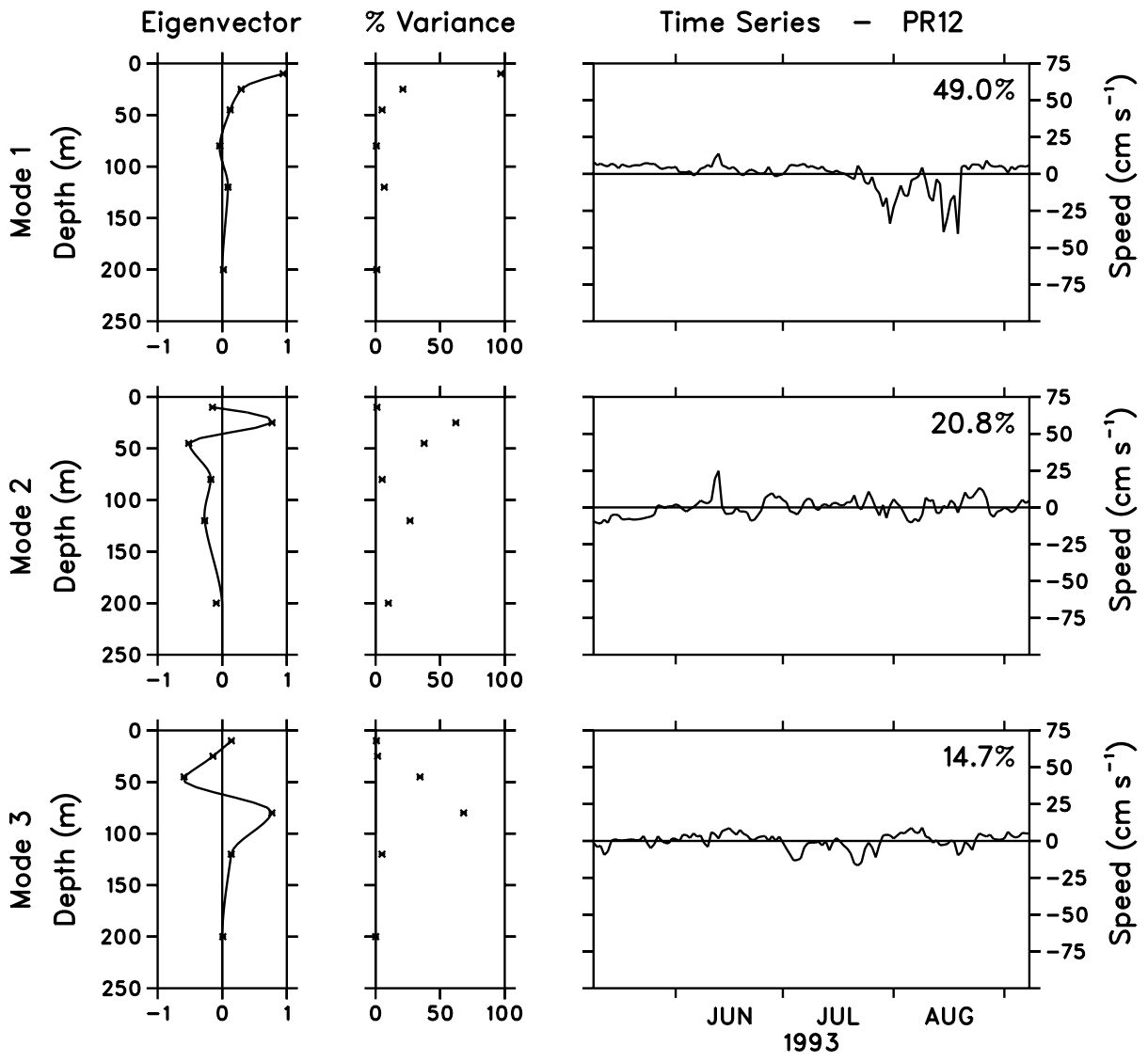

Fig. 17. The first three EOF eigenvectors and time series of ADCP–MCM speed differences for PR12. Percent variance explained at each depth is shown in the center panel. Percent of total variance explained by each EOF is shown in the upper right hand corner of the time series panel. The symbols (x) indicate values at individual MCM depths; the solid curve through the individual eigenvector values is a spline fit which has been forced to zero at 200 m.

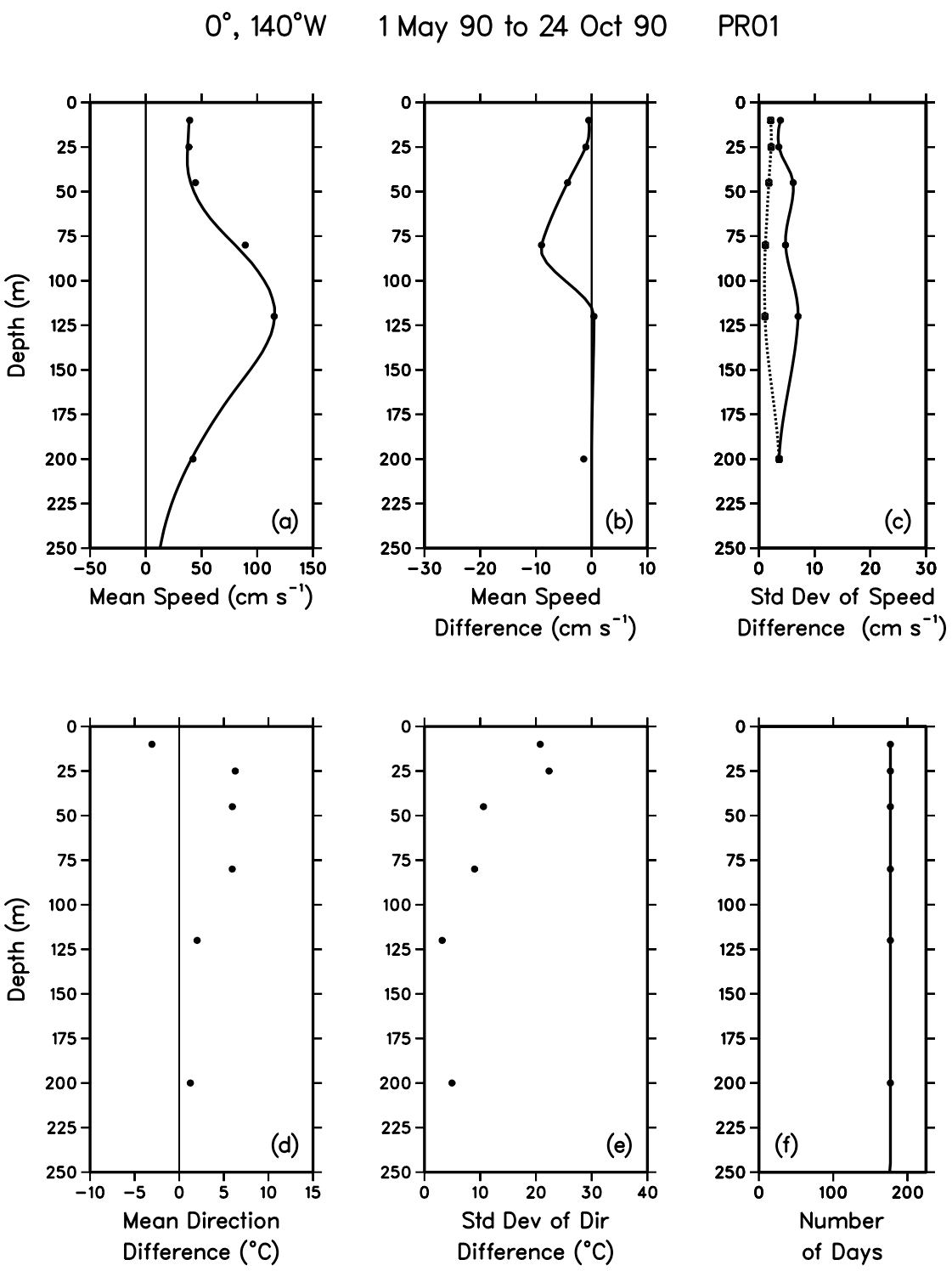

Fig. 18. Profiles of (a) mean speed for MCM data (circles) and ADCP data (solid curve), (b) mean ADCP–MCM speed difference (circles) and spline fit to difference (solid curve), (c) standard deviation of speed difference before EOF correction (solid curve) and after correction (dashed curve), (d) mean ADCP-MCM direction difference, (e) standard deviation of direction difference, and (f) number of days of data collected for MCM (circles) and ADCP (solid curve).

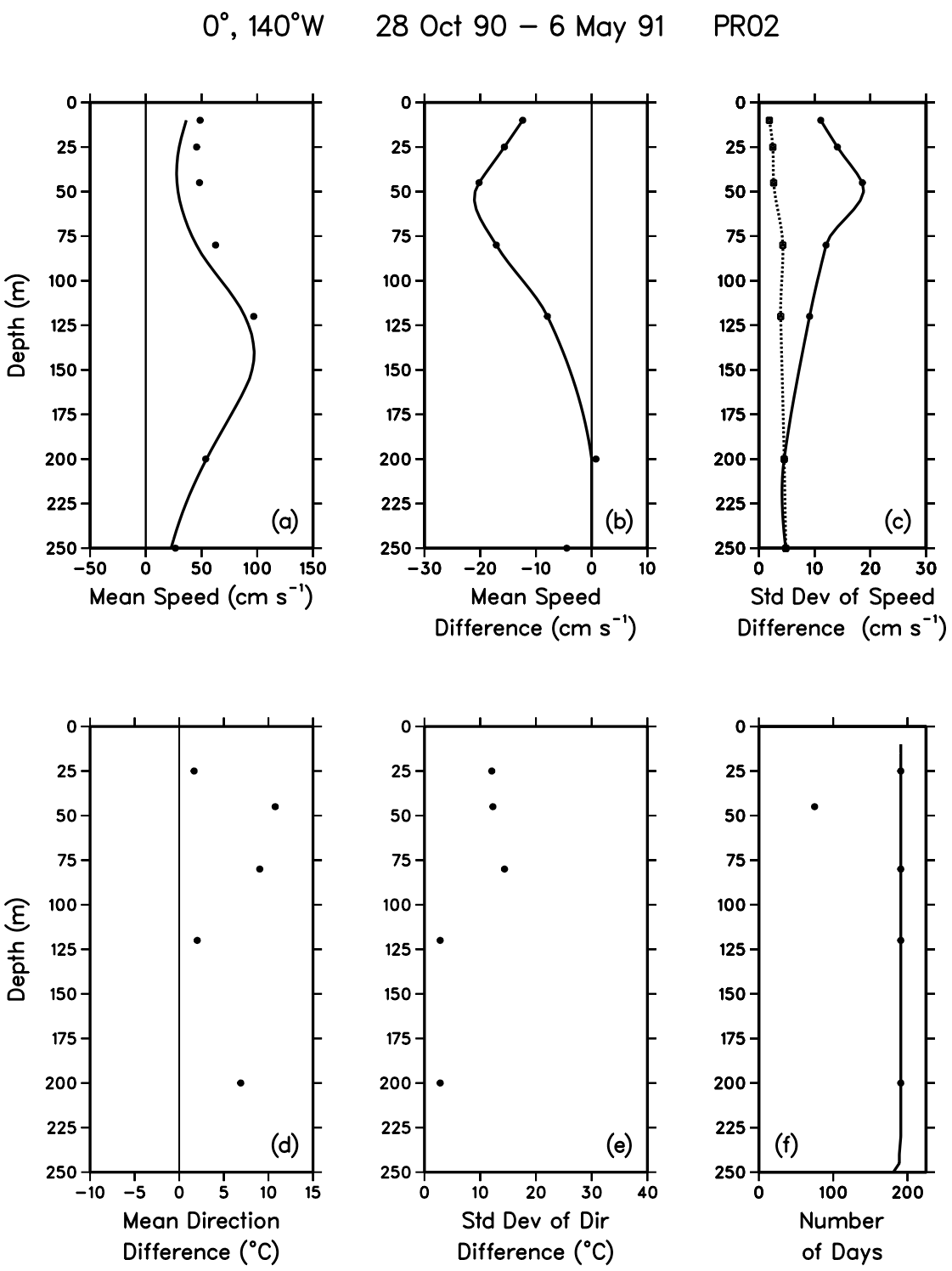

Fig. 19. Profiles of (a) mean speed for MCM data (circles) and ADCP data (solid curve), (b) mean ADCP–MCM speed difference (circles) and spline fit to difference (solid curve), (c) standard deviation of speed difference before EOF correction (solid curve) and after correction (dashed curve), (d) mean ADCP–MCM direction difference, (e) standard deviation of direction difference, and (f) number of days of data collected for MCM (circles) and ADCP (solid curve).

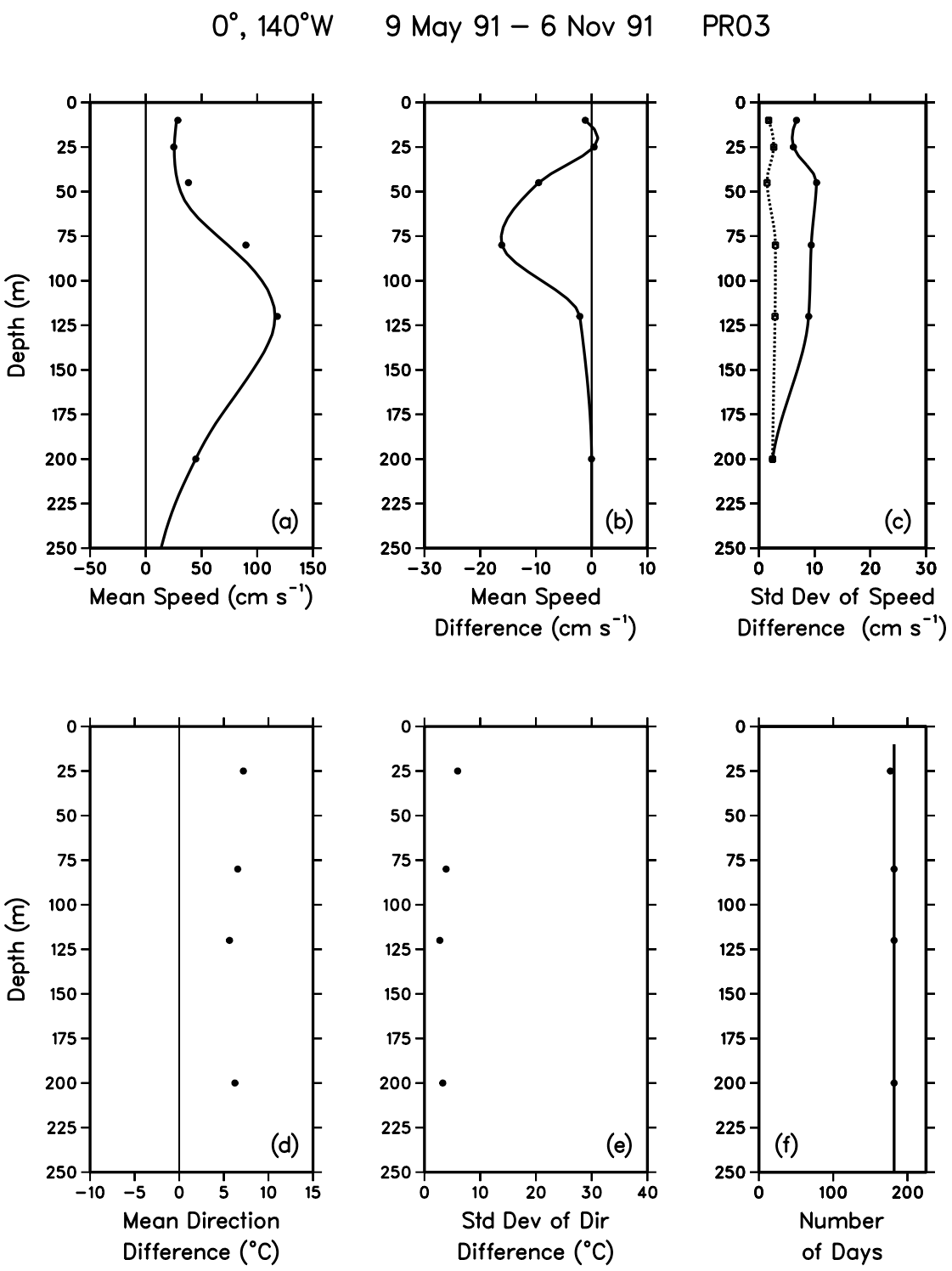

Fig. 20. Profiles of (a) mean speed for MCM data (circles) and ADCP data (solid curve), (b) mean ADCP–MCM speed difference (circles) and spline fit to difference (solid curve), (c) standard deviation of speed difference before EOF correction (solid curve) and after correction (dashed curve), (d) mean ADCP–MCM direction difference, (e) standard deviation of direction difference, and (f) number of days of data collected for MCM (circles) and ADCP (solid curve).

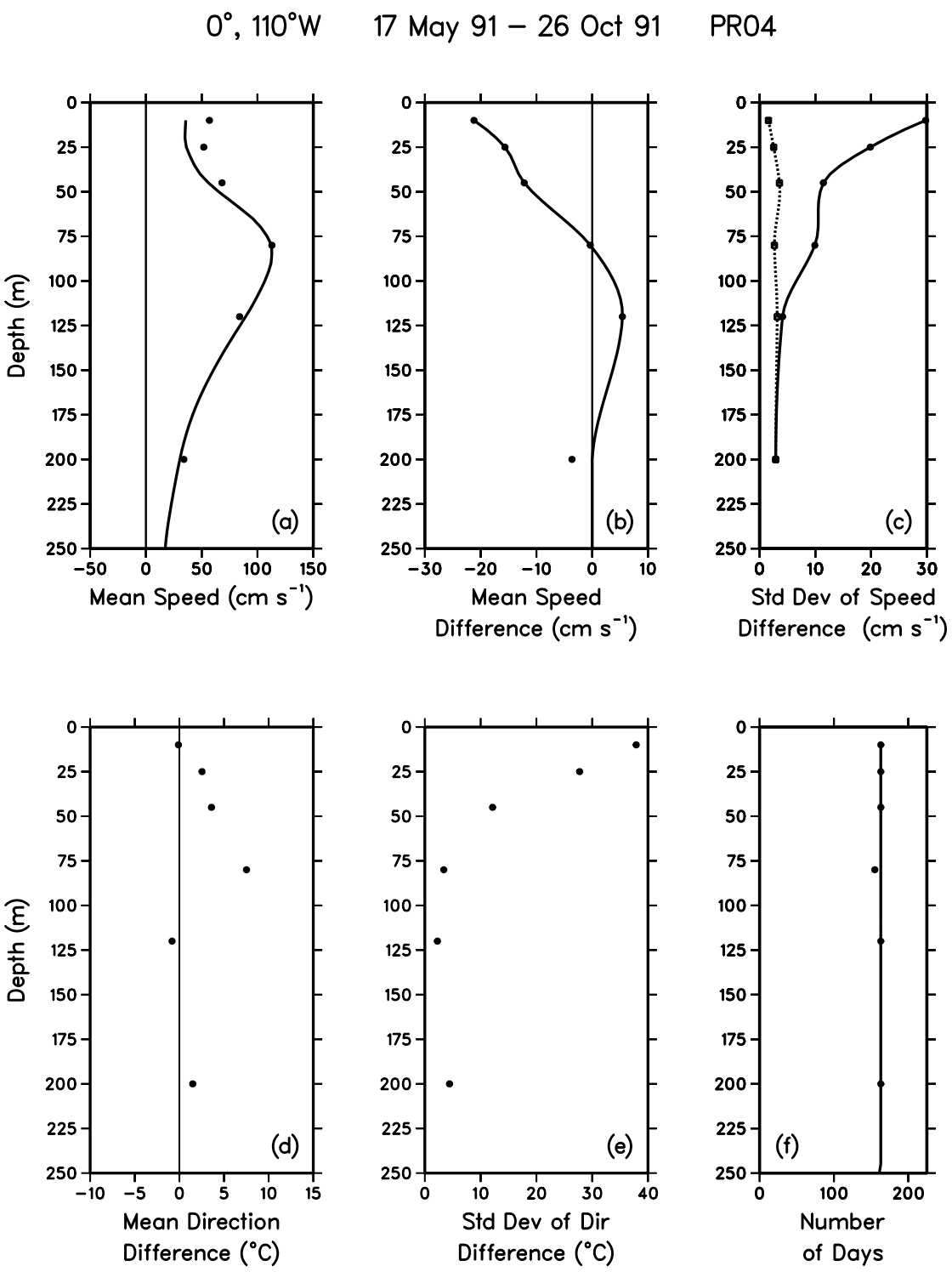

Fig. 21. Profiles of (a) mean speed for MCM data (circles) and ADCP data (solid curve), (b) mean ADCP–MCM speed difference (circles) and spline fit to difference (solid curve), (c) standard deviation of speed difference before EOF correction (solid curve) and after correction (dashed curve), (d) mean ADCP–MCM direction difference, (e) standard deviation of direction difference, and (f) number of days of data collected for MCM (circles) and ADCP (solid curve).

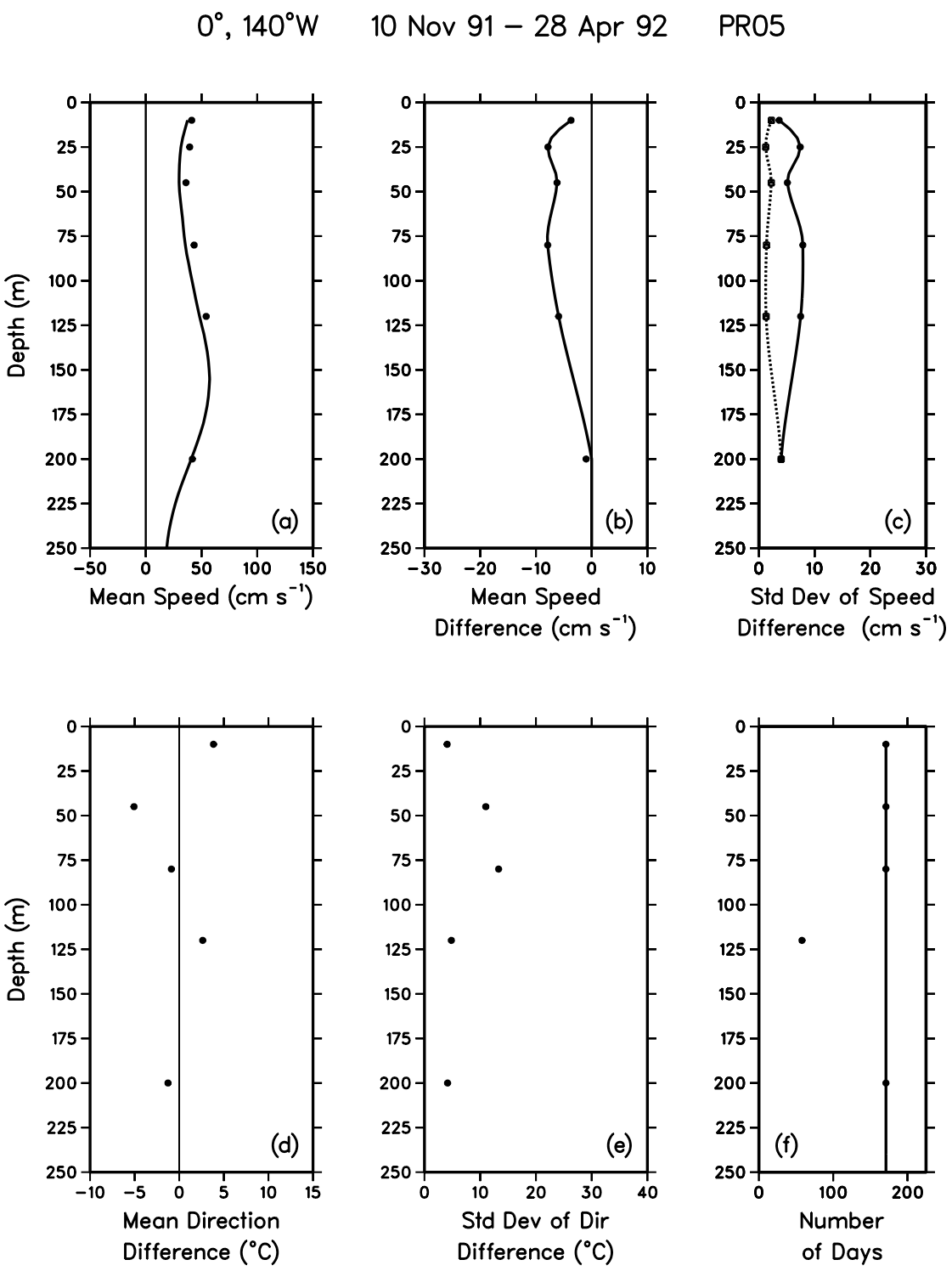

Fig. 22. Profiles of (a) mean speed for MCM data (circles) and ADCP data (solid curve), (b) mean ADCP–MCM speed difference (circles) and spline fit to difference (solid curve), (c) standard deviation of speed difference before EOF correction (solid curve) and after correction (dashed curve), (d) mean ADCP–MCM direction difference, (e) standard deviation of direction difference, and (f) number of days of data collected for MCM (circles) and ADCP (solid curve).

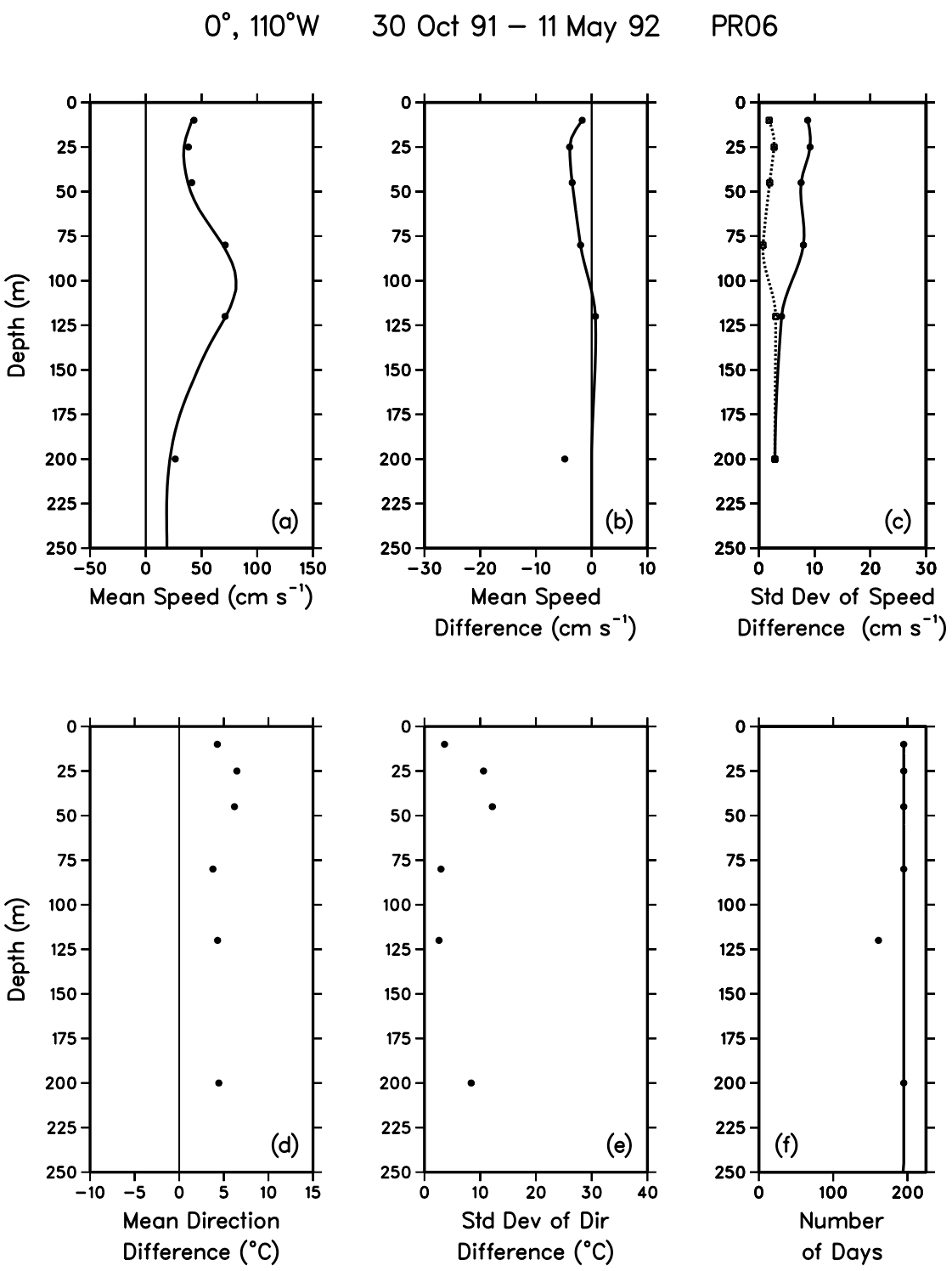

Fig. 23. Profiles of (a) mean speed for MCM data (circles) and ADCP data (solid curve), (b) mean ADCP–MCM speed difference (circles) and spline fit to difference (solid curve), (c) standard deviation of speed difference before EOF correction (solid curve) and after correction (dashed curve), (d) mean ADCP–MCM direction difference, (e) standard deviation of direction difference, and (f) number of days of data collected for MCM (circles) and ADCP (solid curve).

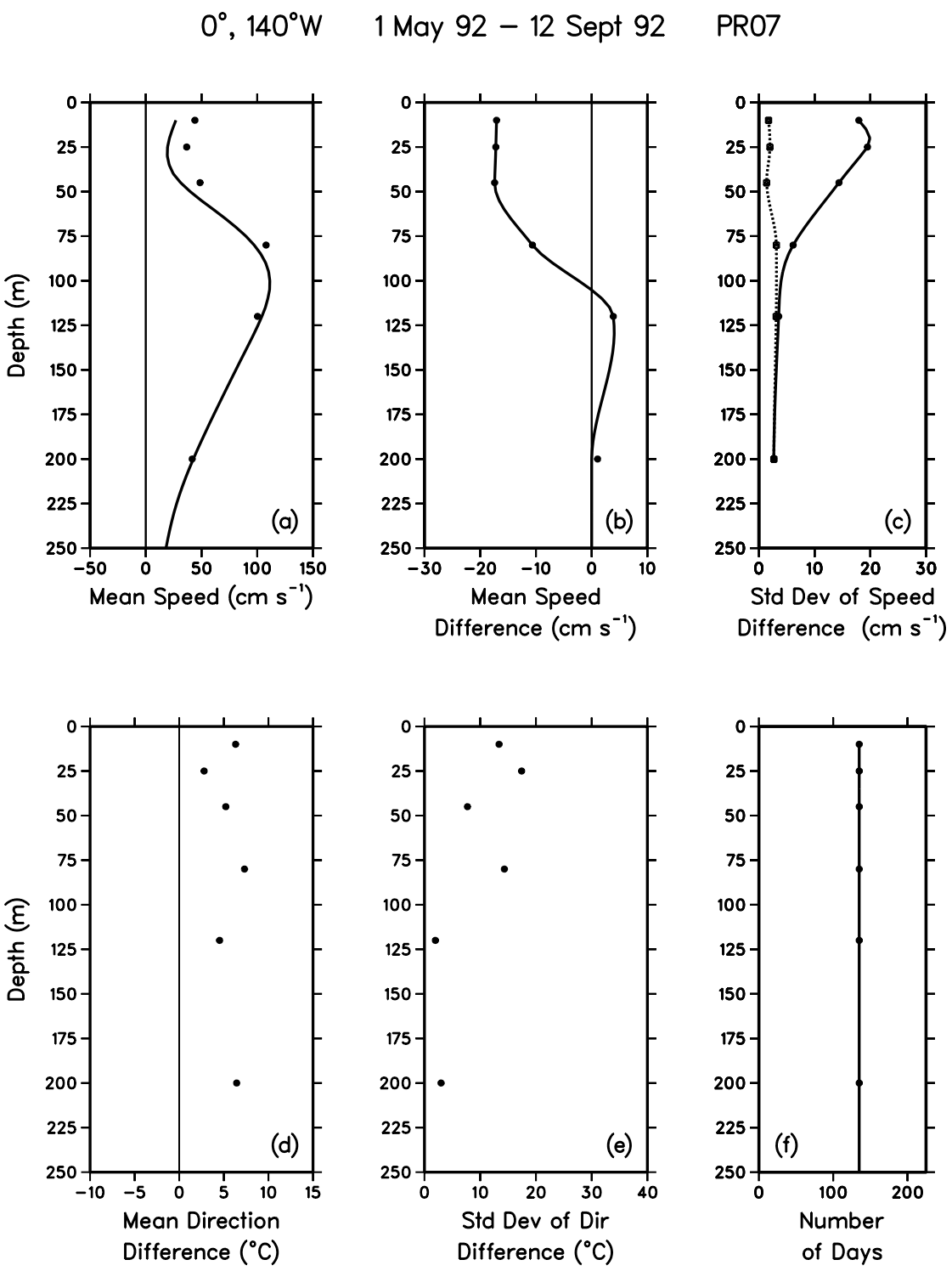

Fig. 24. Profiles of (a) mean speed for MCM data (circles) and ADCP data (solid curve), (b) mean ADCP–MCM speed difference (circles) and spline fit to difference (solid curve), (c) standard deviation of speed difference before EOF correction (solid curve) and after correction (dashed curve), (d) mean ADCP–MCM direction difference, (e) standard deviation of direction difference, and (f) number of days of data collected for MCM (circles) and ADCP (solid curve).

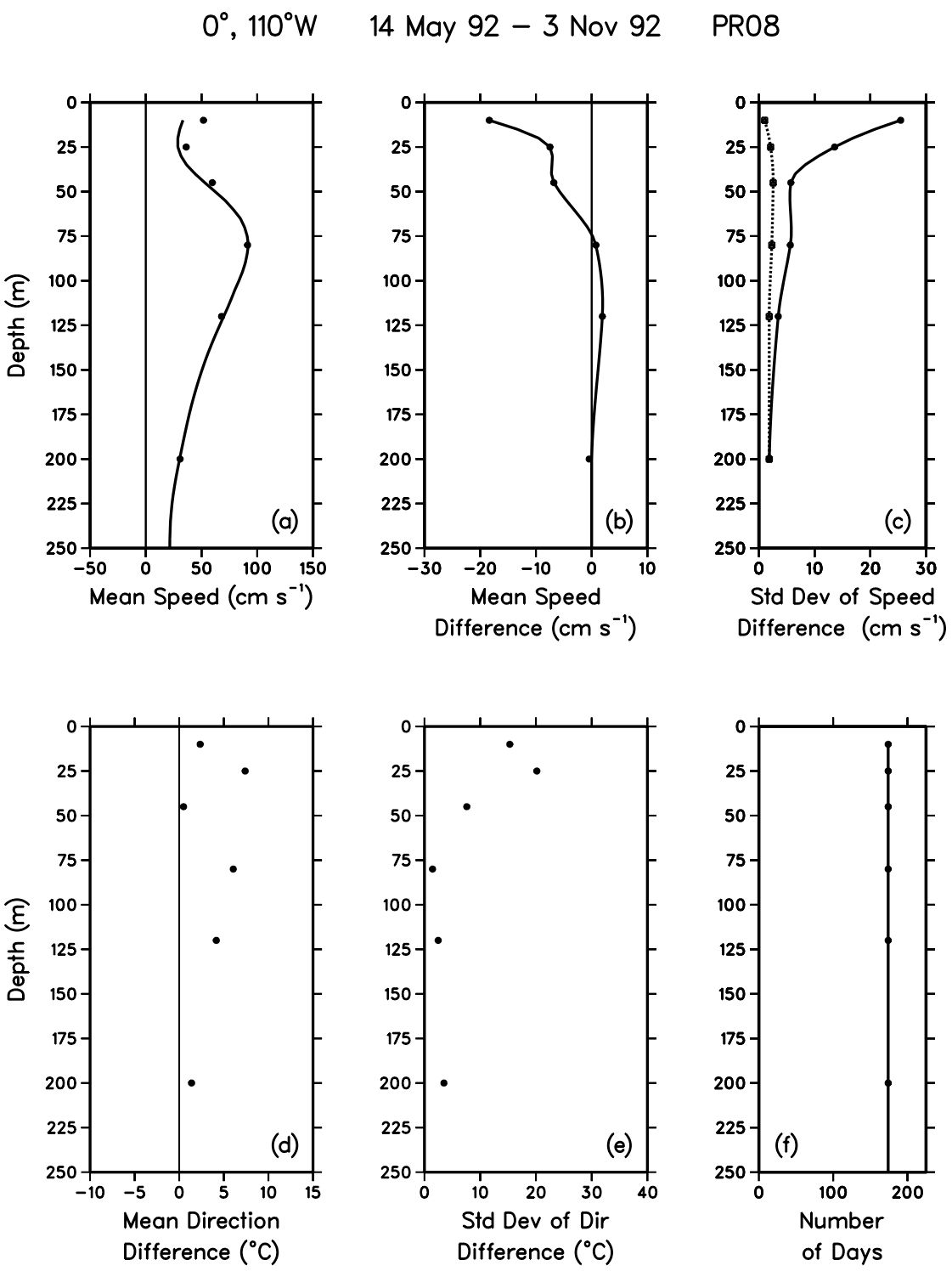

Fig. 25. Profiles of (a) mean speed for MCM data (circles) and ADCP data (solid curve), (b) mean ADCP–MCM speed difference (circles) and spline fit to difference (solid curve), (c) standard deviation of speed difference before EOF correction (solid curve) and after correction (dashed curve), (d) mean ADCP–MCM direction difference, (e) standard deviation of direction difference, and (f) number of days of data collected for MCM (circles) and ADCP (solid curve).

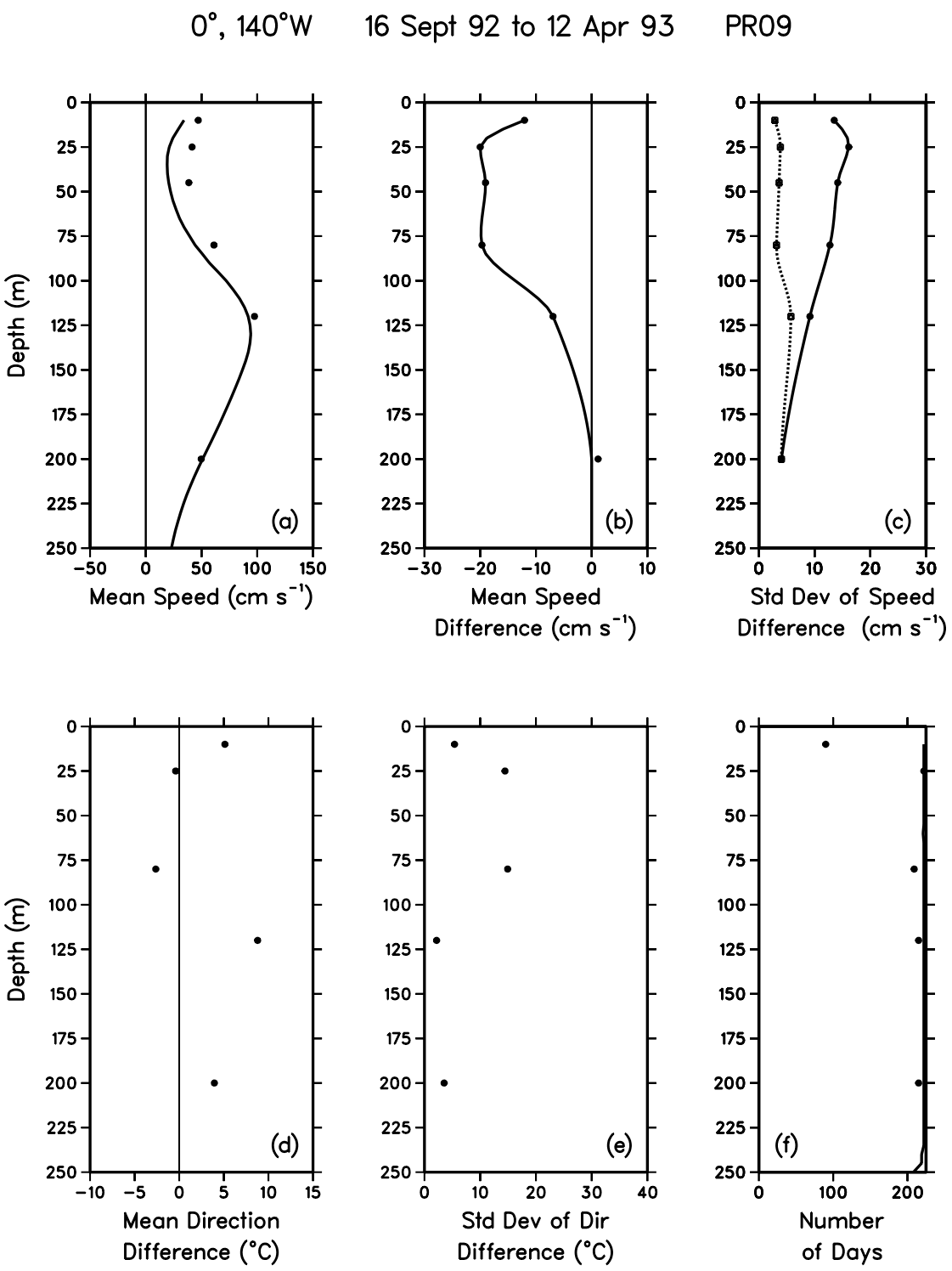

Fig. 26. Profiles of (a) mean speed for MCM data (circles) and ADCP data (solid curve), b) mean ADCP–MCM speed difference (circles) and spline fit to difference (solid curve), (c) standard deviation of speed difference before EOF correction (solid curve) and after correction (dashed curve), (d) mean ADCP–MCM direction difference, (e) standard deviation of direction difference, and (f) number of days of data collected for MCM (circles) and ADCP (solid curve).

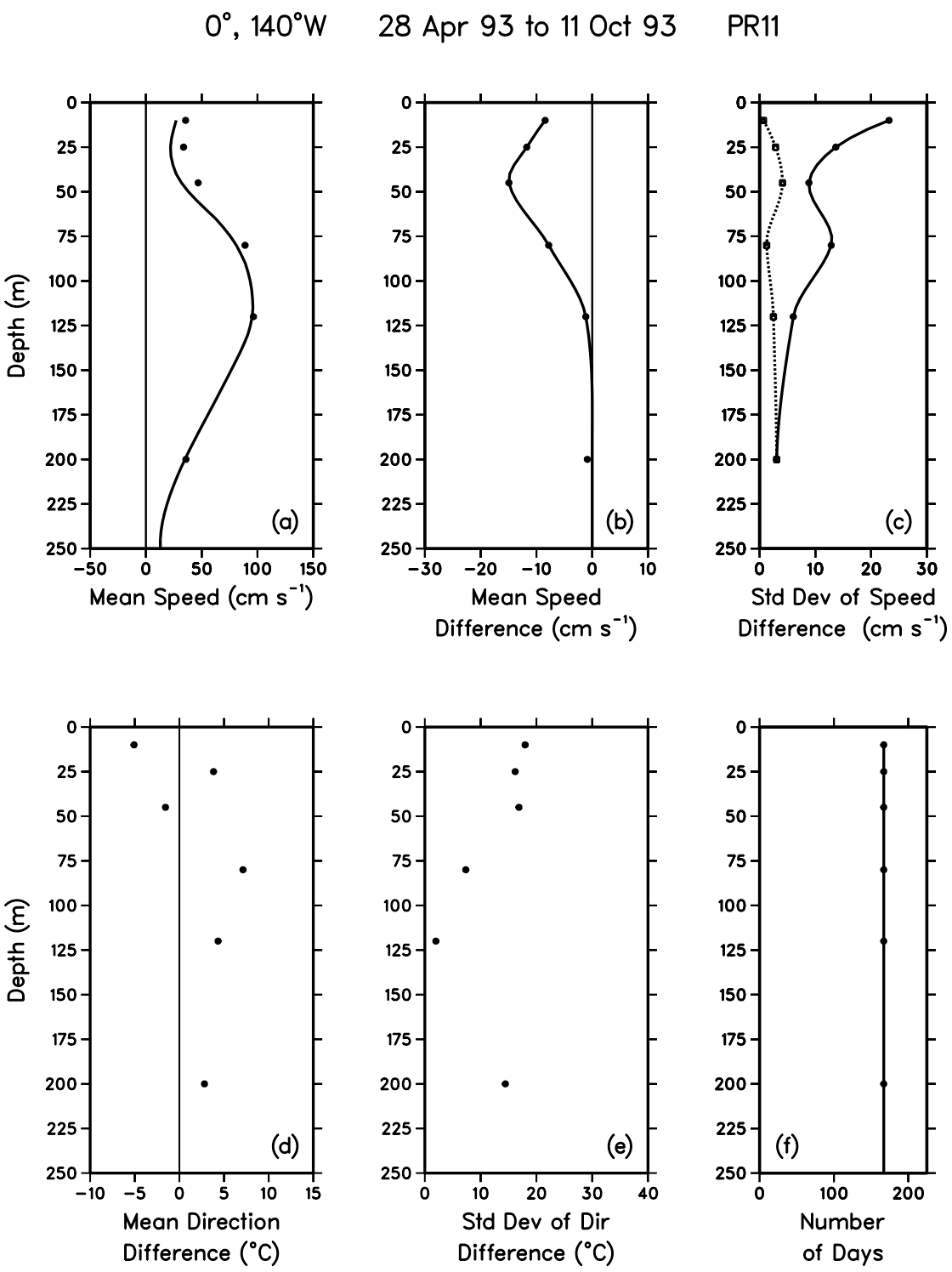

Fig. 27. Profiles of (a) mean speed for MCM data (circles) and ADCP data (solid curve), (b) mean ADCP–MCM speed difference (circles) and spline fit to difference (solid curve), (c) standard deviation of speed difference before EOF correction (solid curve) and after correction (dashed curve), (d) mean ADCP–MCM direction difference, (e) standard deviation of direction difference, and (f) number of days of data collected for MCM (circles) and ADCP (solid curve).

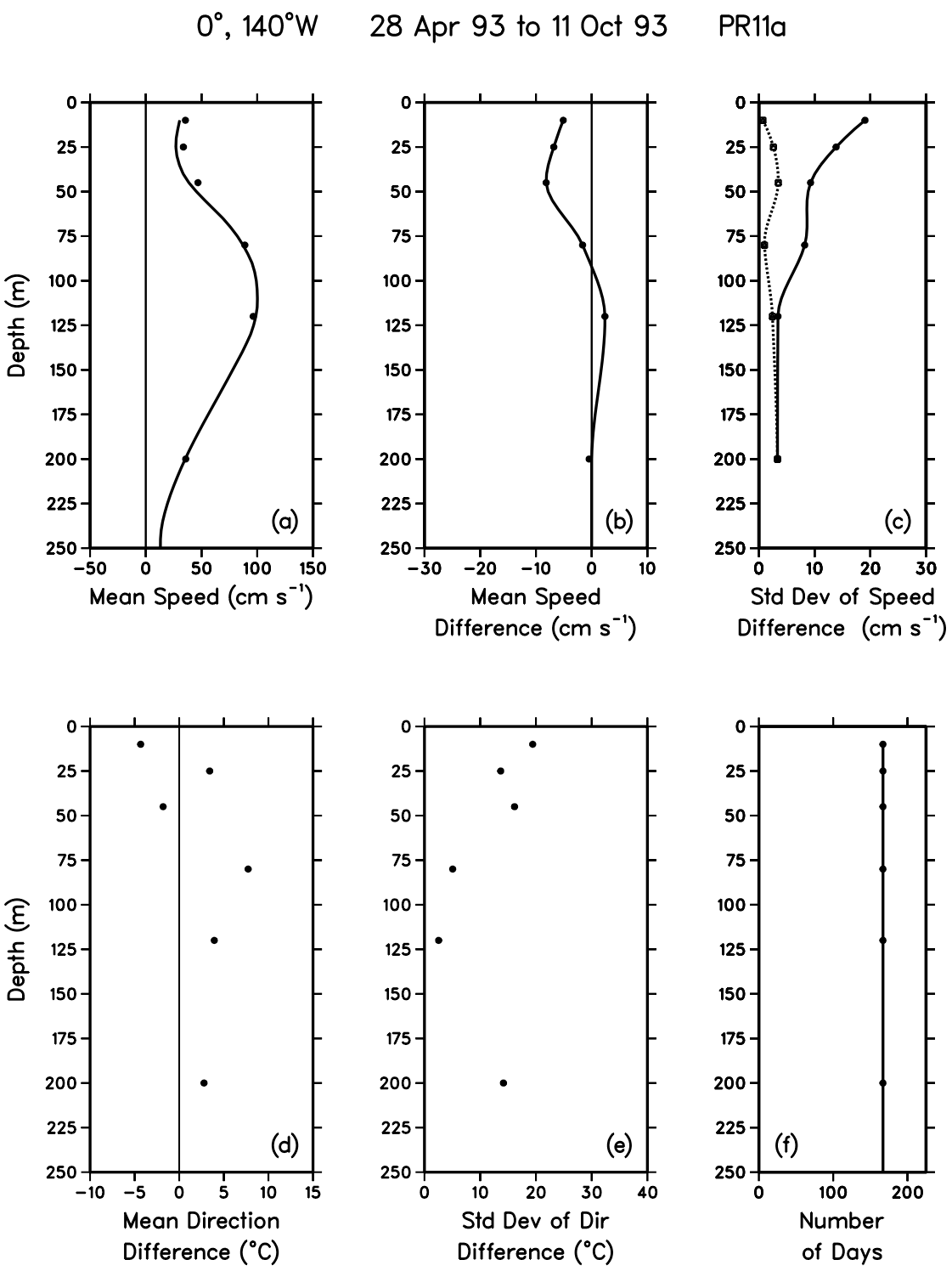

Fig. 28. Profiles of (a) mean speed for MCM data (circles) and ADCP data (solid curve), (b) mean ADCP–MCM speed difference (circles) and spline fit to difference (solid curve), (c) standard deviation of speed difference before EOF correction (solid curve) and after correction (dashed curve), (d) mean ADCP–MCM direction difference, (e) standard deviation of direction difference, and (f) number of days of data collected for MCM (circles) and ADCP (solid curve).

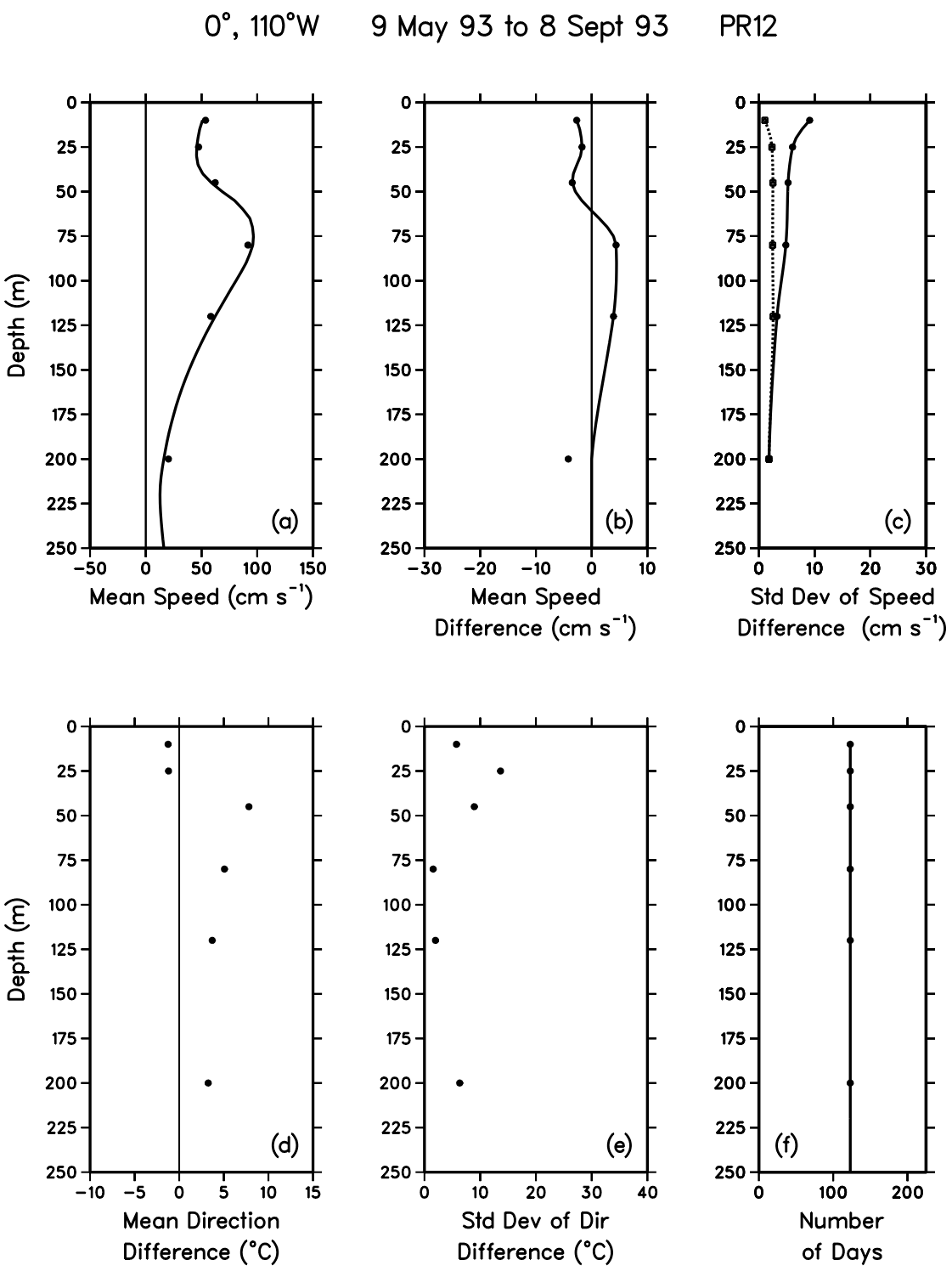

Fig. 29. Profiles of (a) mean speed for MCM data (circles) and ADCP data (solid curve), (b) mean ADCP–MCM speed difference (circles) and spline fit to difference (solid curve), (c) standard deviation of speed difference before EOF correction (solid curve) and after correction (dashed curve), (d) mean ADCP–MCM direction difference, (e) standard deviation of direction difference, and (f) number of days of data collected for MCM (circles) and ADCP (solid curve).

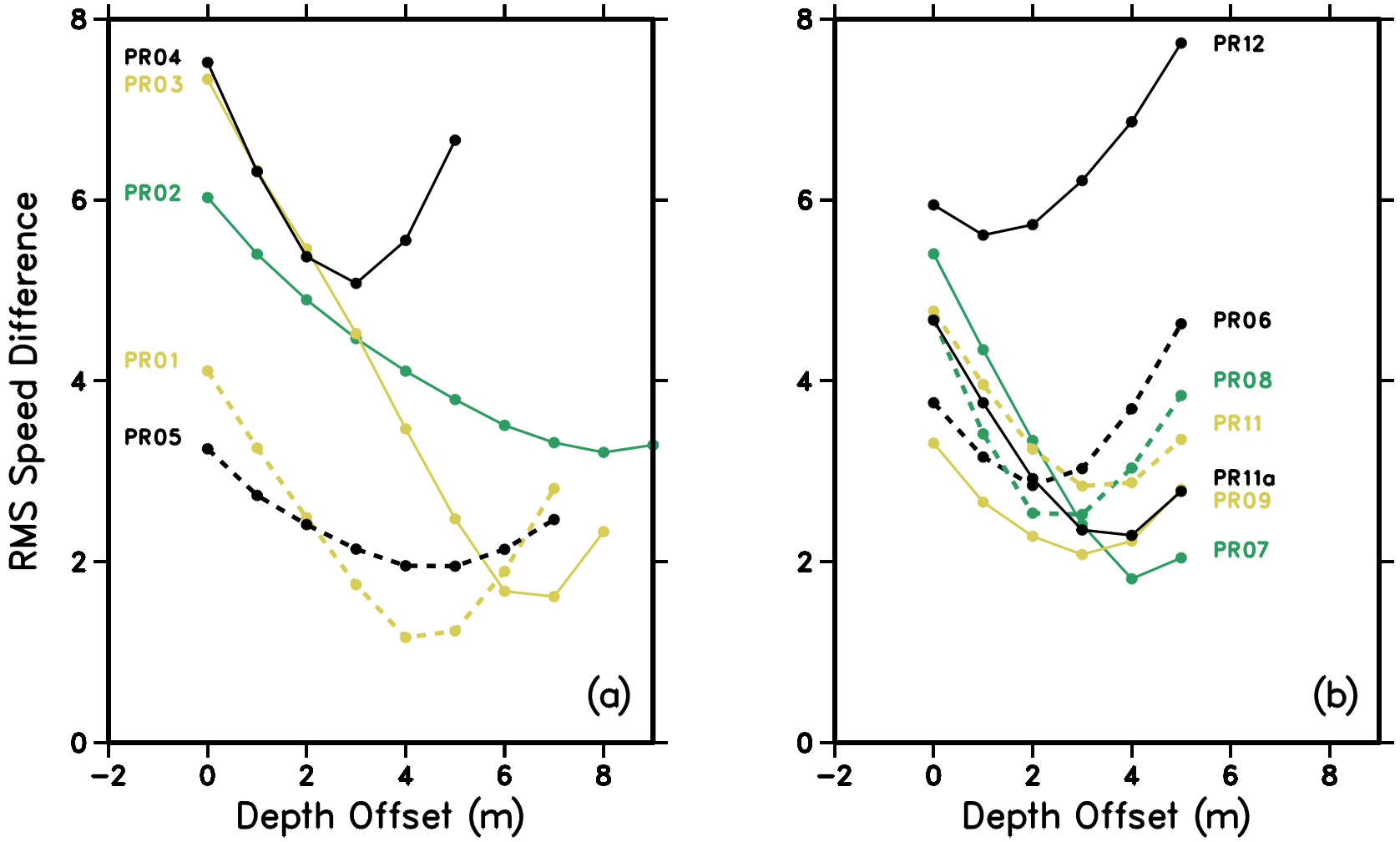

Fig. 30. RMS speed difference between ADCP and MCM data versus depth offset for the first 2 weeks of each deployment. The ADCP data were remapped in progressively shallower 1-m offsets for the comparisons. The figures indicate possible depth errors of (a) 3 to 8 m for the early deployments with the narrow bandwidth tracking filter and (b) 1 to 4 m for the later deployments which had a broad bandwith tracking filter to a depth below the Undercurrent core.

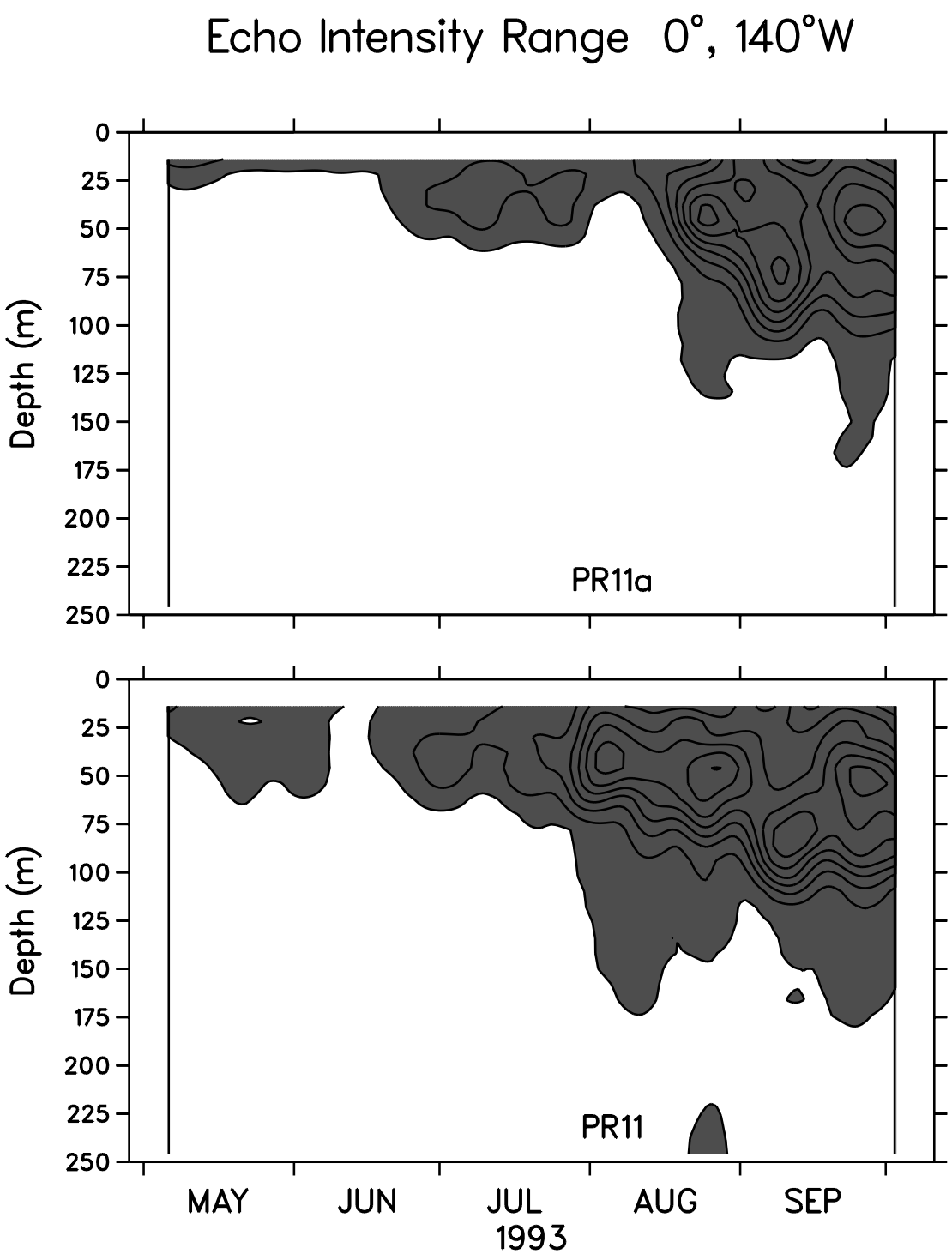

Fig. 31. Contours of echo intensity range for PR11a (no MCMs in the mooring line) and PR11 (with MCMs in the mooring line). Areas greater than 2 db are shaded with 2 db contour levels.

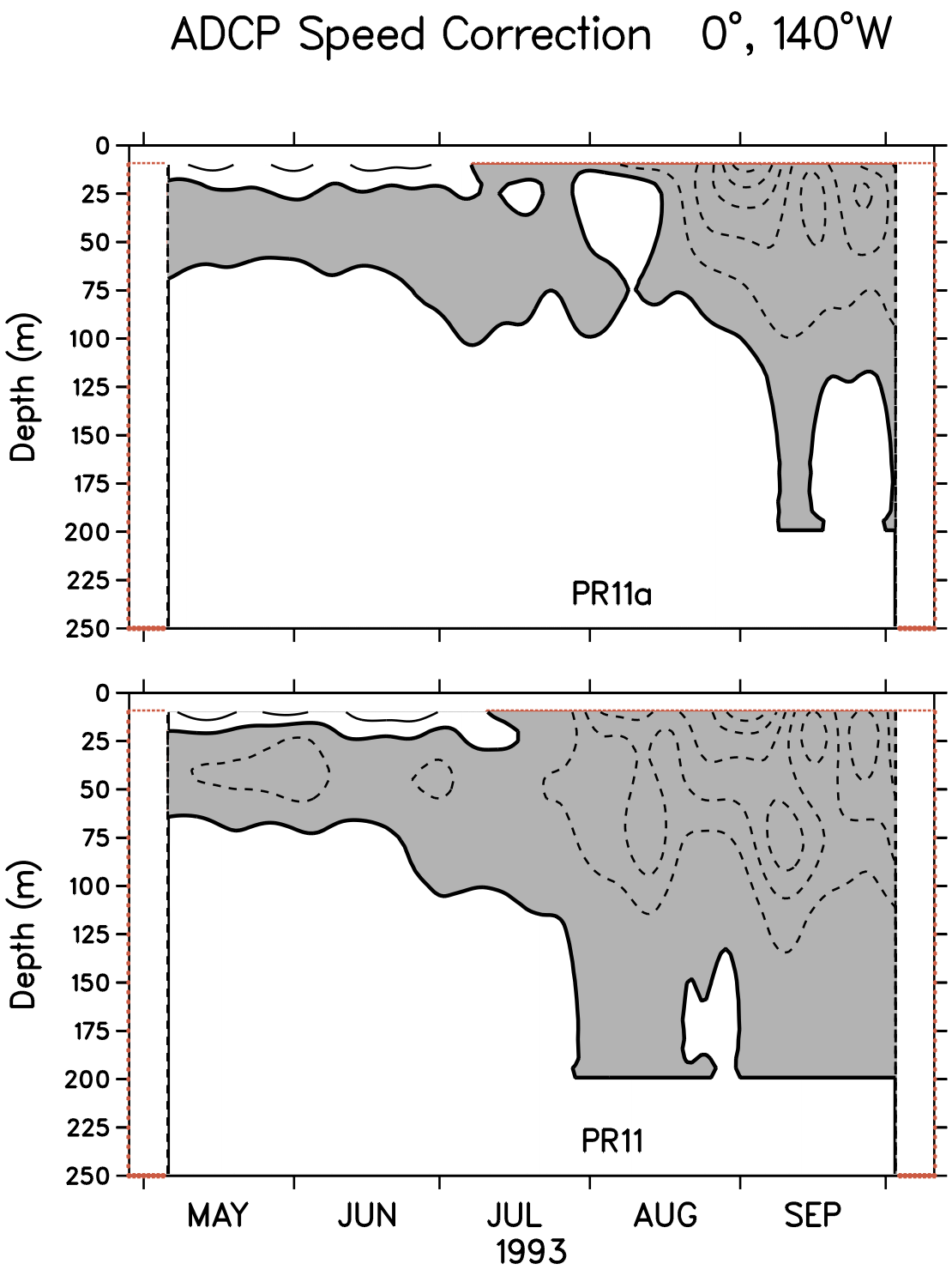

Fig. 32. Contours of ADCP speed correction for PR11a (no MCMs in the mooring line) and PR11 (with MCMs in the mooring line). Shaded areas are negative values with 10 cm s^{-1} contours.

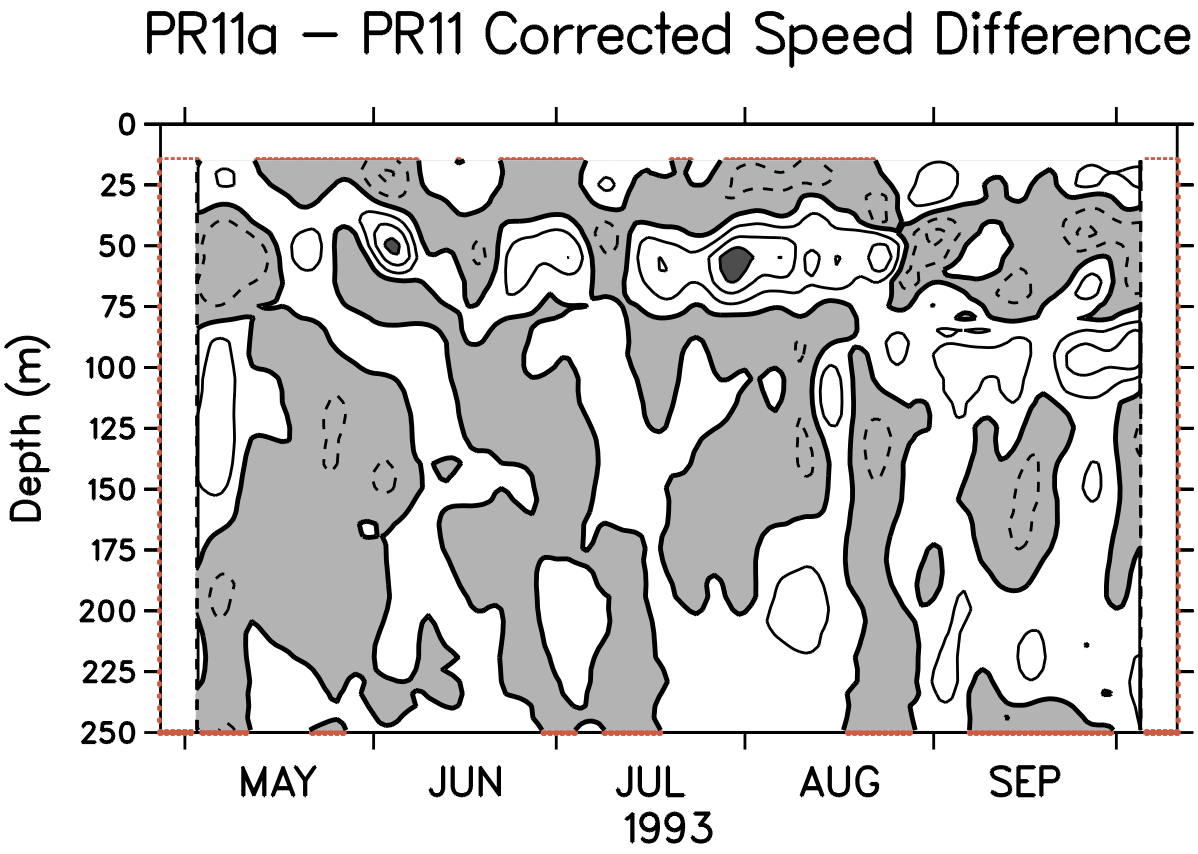

Fig. 33. Contours of daily differences of PR11a–PR11 corrected speeds. Contour intervals are 2 cm s^{-1} with negative values lightly shaded.

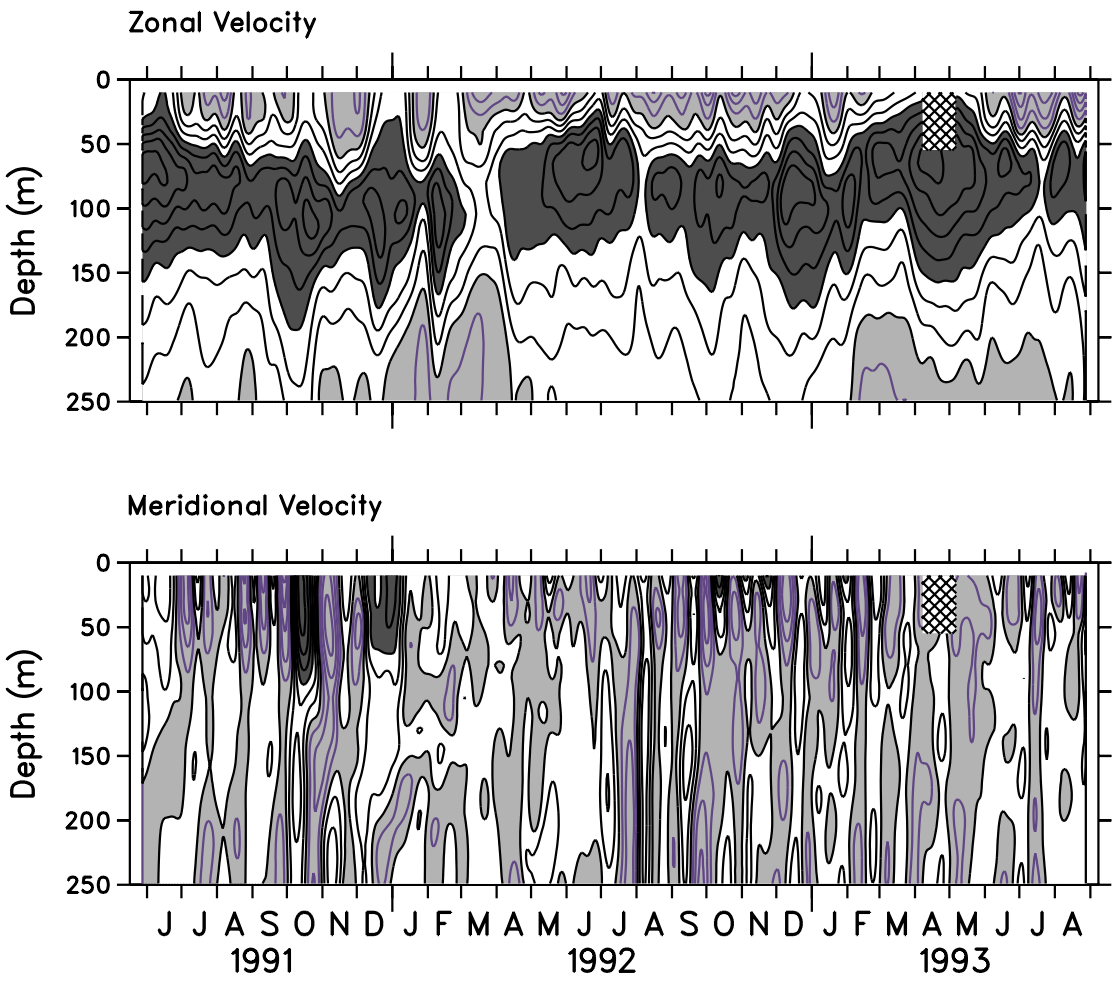

Fig. 34. Zonal and meridional velocity at 0°, 110°W from corrected daily profiles of ADCP data. Contours are 20 cm s^{-1} with light shading for westward and southward velocities. Dark shading represents eastward or northward velocities greater than 60 cm s^{-1}. Areas of missing data are crosshatched.

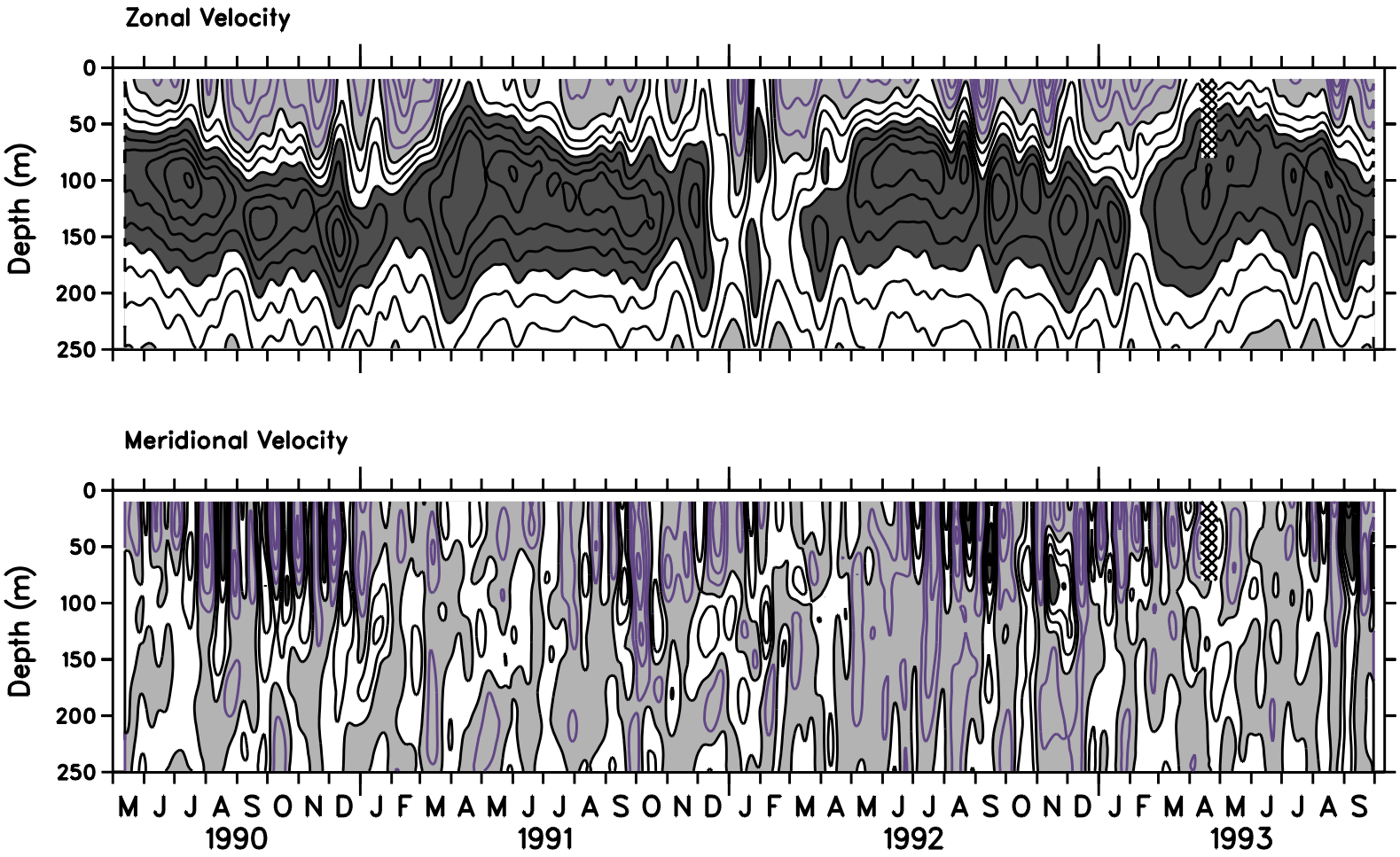

Fig. 35. Zonal and meridional velocity at 0°, 140°W from corrected daily profiles of ADCP data. Contours are 20 cm s^{-1} with light shading for westward and southward velocities. Dark shading represents eastward or northward velocities greater than 60 cm s^{-1}. Areas of missing data are crosshatched.